UTRECHT UNIVERSITY

INSTITUTE OF MARINE AND ATMOSPHERIC RESEARCH

MSc Thesis

Triple Oxygen Isotope Composition of CO_2: Analytical System Improvements and Seasonal Variability

Yujie Ye

7026390

Supervisors:

Prof. Dr. Thomas Röckmann

Dr. Getachew Adnew

Universiteit Utrecht

July 2022

Abstract

The triple oxygen isotope composition ($\Delta'^{17}O$) of troposphere CO_2 is considered as a potential tracer for quantifying gross primary production (GPP) at an ecosystem scale. In this project, air samples from two different ecosystems, Loobos (evergreen coniferous forest ecosystem) and Cabauw (grassland ecosystem) were taken from December 2020 to April 2022 in order to quantify the seasonal variation in $\Delta'^{17}O$ values of tropospheric CO_2 with the focus of quantifying gross primary production at an ecosystem scale. The $\Delta'^{17}O$ was measured using a CO_2-O_2 isotope exchange technique coupled with an isotope ratio mass spectrometer (IRMS). We characterized and investigated the stability of CO_2-O_2 the isotope exchange system using different CO_2 standards. The results showed that larger thermal diffusion (larger temperature gradients in the CO_2-O_2 isotope exchange reactor) will lead to smaller fractionation both for reactor temperature of 750 ℃ and 1000 ℃. Tropospheric CO_2 sampled in Cabauw has an average $\Delta'^{17}O$ value of 0.221 $\pm$ 0.006‰(SE) from December 2020 to April 2022. The temporal evaluation of $\Delta'^{17}O$ values does not show a clear seasonal cycle with slight upward trend toward summer but more scattered in the winter, with an amplitude of approximately 0.08‰. The seasonal variation of $\Delta'^{17}O$ value of tropospheric CO_2 and its upward trend toward summer indicate the activity of terrestrial vegetation and may be used as a potential tracer of GPP.

1 Introduction

The carbon cycle controls the relative distribution of emitted carbon dioxide between the atmosphere, land surface, and oceans. There are several sinks for CO_2, for example, atmospheric CO_2 can be taken up by plants, ocean and soil. And there are several sources for CO_2, for example, fossil fuel burning (from some energy and industrial processes) and land use change (such as deforestation, change in agricultural practices). About three-quarters of anthropogenic CO_2 emissions are due to fossil fuel burning. (Prentice et al., 2001)

Figure 1 illustrates the present understanding of the global atmospheric carbon cycle. Atmospheric CO_2 emissions are rising at a rate of 4.7 ± 0.1 PgC/yr. The Ocean sink for CO_2 increased to 2.4 ± 0.5 PgC/yr from 2008-2017. Terrestrial biosphere sinks for CO_2 (differences between total respiration and total photosynthetic fluxes) increased to 3.2 ± 0.7 PgC/yr from 2008-2017. Global fossil CO_2 emissions increased on average to 9.4 ± 0.5 PgC/yr over the period 2008-2017. CO_2 emissions due to land use change are around 1.5 ± 0.7 PgC/yr. (Le Quéré et al., 2018; Joiner et al., 2018)

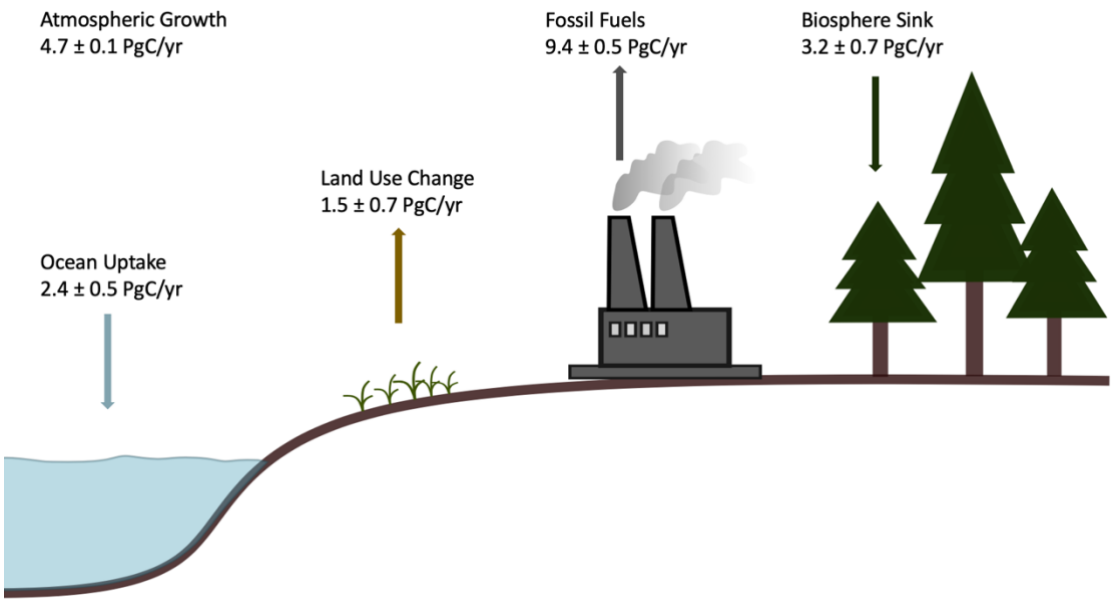

Figure 1: A simplified schematic of the global carbon cycle over the period 2008-2017 adapted from Joiner et al., 2018. The carbon exchange fluxes are represented in PgC/yr.

Gross primary production (GPP) refers to the total amount of carbon dioxide (CO_2) fixed by plants in the ecosystem per unit time through photosynthesis. GPP plays a key role in the global carbon cycle as it regulates the amount of anthropogenic CO_2 in the atmosphere (Joiner et al., 2018) and the terrestrial biosphere accounts for about half of the global net carbon sink of anthropogenic CO_2. (Hoag et al., 2005)

Increasing the understanding of terrestrial carbon cycle and its uncertainty is important for predicting future temperatures and atmospheric CO_2 concentrations, (Booth et al., 2012) especially under the risk of global warming nowadays. However, in the absence of direct observations, only preliminary observational estimates of global terrestrial GPP can be made so far. (Beer et al., 2010) Moreover, large uncertainties remain due to the spatial and temporal variability of the emissions and the representativity of the observational system. (Gurney et al., 2002)

Observations and investigation of the $\delta^{18}O$ signal (the ratio of isotope ^{18}O to ^{16}O) in tropospheric CO_2 has been of interest in studying the global carbon cycle since $\delta^{18}O$ is dominated by CO_2 exchange (both photosynthetic uptake and respiration) with the terrestrial biosphere (Ciais et al., 1997; Farquhar et al., 1993). When atmospheric CO_2 is assimilated as it enters the leaves, the water in the leaves exchange isotopes with CO_2, and when the rest of the CO_2 diffuses out to the atmosphere, the new $\delta^{18}O$ value is determined largely by the $\delta^{18}O$ of the water in the leaves. (Farquhar et al. 1993; Francey & Tans 1987) Therefore the signal of new CO_2 can be a tracer to estimate gross primary production at an ecosystem scale.

Using $\delta^{18}O$ as the tracer for CO_2 fluxes still have some limitation. $\delta^{18}O$ value is determined by various water reservoirs and different environmental conditions, such as leaf water, vertical distribution in soils, humidity in the canopy, numerous different water surfaces and other factors such as precipitation and temperature. Apart from these, it also depends on time and space. It requires measurement and accurate estimation of $\delta^{18}O$ values for all these numerous water reservoirs, which is difficult to obtain. (Hoag et al., 2005).

In order to overcome the limitation of using $\delta^{18}O$, the difference between the amounts of $\delta^{18}O$ and $\delta^{17}O$ of tropospheric CO_2, which is defined as the $\Delta'^{17}O$ (CO_2) (triple oxygen composition in CO_2), has been considered as a potential new tracer for terrestrial gross carbon fluxes (Hoag et al., 2005). And it also has been used by many studies to be a tracer to study the CO_2 fluxes between the biosphere and the atmosphere (e.g. Luz et al., 1999; Liang et al., 2017; Koren et al., 2019). It has been suggested that $\Delta'^{17}O$ is a better tracer for terrestrial gross carbon fluxes than $\delta^{18}O$ alone, since $\delta^{18}O$ value is determined largely by various water reservoirs, such as leaf water, which is difficult to obtain and measure.(Hoag et al., (2005) This is also the case for $\Delta'^{17}O$, however, $\Delta'^{17}O$ signal depends much less on various water reservoirs compared to $\delta^{18}O$, also the $\Delta'^{17}O$ signal is much smaller than $\delta^{18}O$. Therefore, we do not need complex measurements to obtain accurate estimates of $\delta^{18}O$ for various water reservoirs, and easier to connect to GPP.

The aim of this project is to quantify the seasonal variation in $\Delta'^{17}O$ of tropospheric CO_2 in two different ecosystems as a tool for quantifying gross primary production at an ecosystem scale. The analysis of $\Delta'^{17}O$ was carried out using an $\Delta'^{17}O$ measurement system including isotope ratio mass spectrometry and CO_2-O_2 isotope exchange techniques. Here we followed the methods of CO_2-O_2 isotope exchange technique described by Adnew et al., (2019). In the first part of the thesis, several experiments were performed in order to characterize the system and investigate the stability and potential internal effects of CO_2-O_2 isotope exchange system, including equilibrium reaction times for CO_2-O_2 exchange reactions at different reactor pressures, effect of temperature gradients in the reactor on the fractionation of the CO_2-O_2 isotope exchange reaction, different reaction temperature, potential isotope exchange with molecular sieve, silica gel and the quartz reactor, and we also investigated the accuracy and stability of the isotope ratio mass spectrometer. In the second part of this thesis, the air samples collected through the whole year from Cabauw and Loobos were measured by the CO_2-O_2 isotope exchange system to quantify the seasonal variation in ^{13}C, ^{18}O and $\Delta'^{17}O$ value of troposphere CO_2.

2 Theory

2.1 Theory of oxygen isotopes

Oxygen has three stable isotopes, namely ^{16}O, ^{17}O, and ^{18}O with an atmospheric abundance of 99.76%, 0.04%, 0.21%, respectively. The most abundant isotopologues of CO_2 primarily include $^{12}C^{16}O^{16}O$, $^{13}C^{16}O^{16}O$, $^{12}C^{17}O^{16}O$, and $^{12}C^{18}O^{16}O$.

	Isotopologues	Abundance
O	^{16}O	99.76%
	^{17}O	0.04%
	^{18}O	0.21%
C	^{12}C	98.89%
	^{13}C	1.11%

Table 1: Abundances of the isotopologues of CO_2

The two isotope ratios for oxygen isotopes can be expressed as $^{18}R = [^{18}O]/[^{16}O]$ and $^{17}R = [^{17}O]/[^{16}O]$. The isotope signature is reported relative to the international reference and expressed in delta notation. For instance, $\delta^{18}O$, is reported relative to Vienna Standard Mean Ocean Water (VSMOW) as shown in equation 1.

$$\delta^{18}O = \frac{[^{18}O/^{16}O]_{sample}}{[^{18}O/^{16}O]_{VSMOW}} - 1 \qquad (2.1)$$

δ values are normally expressed in per mill (‰).

2.2 Definition of Δ'^{17}O

Stratospheric photochemistry leads to ^{17}O enrichments in CO_2 higher than what is expected from mass dependent fractionation processes. This ^{17}O-enrichement of CO_2 results from isotope selective processes in ozone formation. Photolysis of O_3 produces electronically excited free oxygen radicals, $O(^1D)$, which combine with CO_2 to form the unstable CO_3^*. Finally, the unstable CO_3^* will dissociate into CO_2 and a ground state oxygen atom $O(^3P)$.

$$O_3 + h\nu \rightarrow O_2 + O(^1D) \tag{2.2}$$

$$O(^1D) + CO_2 \rightarrow CO_3^* \rightarrow CO_2 + O(^3P) \tag{2.3}$$

This ^{17}O- enrichments in CO_2 can be expressed as

$$\Delta'^{17}O\ (CO_2) = \ln(\delta^{17}O + 1) - \lambda \ln(\delta^{18}O + 1) \neq 0 \tag{2.4}$$

where λ is the three isotope slope for oxygen isotope fractionation. λ can range from 0.5 to 0.5305 for individual fractionation processes. In this study, a reference λ value is chosen as 0.528 to calculate $\Delta'^{17}O\ (CO_2)$ according to Luz and Barkan, 2010; Meijer and Li, 1998. $\Delta^{17}O$ values are reported in ‰.

Therefore, in the upper troposphere, there is a stratospheric CO_2 inflow of $\Delta'^{17}O \gg 0‰$. Then CO_2 will come into contact with liquid water in terrestrial biosphere, including vegetation, soils, or oceans. When CO_2 is dissolved in liquid H_2O, the CO_2 isotope composition will be reset to be in isotope equilibrium with the water isotope composition. Therefore, the CO_2 released back to the atmosphere after contacting a water body has a signature of $\Delta'^{17}O \approx 0‰$.

3 Method

The $\Delta'^{17}O$ value of CO_2 cannot be measured directly, because $^{13}C^{16}O^{16}O$ (mass 44.993) and $^{12}C^{17}O^{16}O$ (mass 44.994) have almost the same molecular mass of nearly 45, so it is not possible to distinguish them since the difference between them exceeds the resolving power of typical isotope ratio mass spectrometers, and even the newly developed high mass resolution mass spectrometers like the 253 Ultra (Adnew et al., 2019). Due to this mass interference, we need to measure $\delta^{17}O$ using indirect methods.

Several techniques have been developed to measure $\Delta'^{17}O$ values of CO_2 (See Adnew et al., 2020) for an overview). In this thesis I will use a technique based on complete isotope exchange between CO_2 that was developed by Mahata et al (2013) and has been established in several isotope laboratories (Barkan et al., 2015; Adnew et al., 2019) The big strength is that it allows determination of $\Delta'^{17}O$ with a precision better than 0.01 ‰. CO_2 of the air sample and O_2 with known isotope composition are admitted to a reactor volume where they exchange isotopes over a platinum catalyst at high reaction temperature until an isotopic equilibrium is established. After reaching the equilibrium state, the change in isotope composition of O_2 can be measured by isotope ratio mass spectrometry without interference from ^{13}C.

3.1 Theoretical calculations for $\Delta'^{17}O$

The method used in this study to measure $\Delta'^{17}O_i$ of CO_2 follows the process described by Adnew et al. (2019). The theoretical calculations of CO_2 - O_2 isotope equilibrium are based on the mass balance equation for the CO_2- O_2 exchange reaction, which means the total amount of ^{17}O and ^{18}O molecules in the initial CO_2 and O_2 and in the final CO_2 and O_2 are the same. The value of $\delta^{17}O_i(CO_2)$ (i represents initial) can be calculated by the following mass balance equation presented by Barkan et al., (2015).

$$\delta^{17}O_i(CO_2) = \frac{1}{\beta}\left[\left(\delta^{17}O_f(O_2)+1\right)(\alpha^{17}\beta+1) - \left(\delta^{17}O_i(O_2)+1\right)\right] - 1 \qquad (3.1)$$

Where β is the molar ratio of change in initial (index i) and final (index f) values of O_2 and CO_2, which can be defined as the equation shown below，

$$\beta = \frac{\delta^{18}O_i(O_2) - \delta^{18}O_f(O_2)}{\delta^{18}O_f(CO_2) - \delta^{18}O_i(CO_2)} \qquad (3.2)$$

The CO_2 and O_2 will not totally reach the same isotope composition so there is still a small deviation between the final isotopic compositions of CO_2 and O_2 after the exchange reaction reach the equilibrium state. The deviation between them is defined as fractionation factors $^{17}\alpha$ and $^{18}\alpha$, which can be expressed as

$$^{17}\alpha\ (CO_2/O_2) = \frac{\delta^{17}O_f(CO_2)+1}{\delta^{17}O_f(O_2)+1} \tag{3.3}$$

$$^{18}\alpha\ (CO_2/O_2) = \frac{\delta^{18}O_f(CO_2)+1}{\delta^{18}O_f(O_2)+1} \tag{3.4}$$

The final value of $\delta^{18}O$ in CO_2 ($\delta^{18}O_f(CO_2)$) can be calculated from $^{18}\alpha$ and $\delta^{18}O_f(O_2)$ according to the following equation,

$$\delta^{18}O_f(CO_2) = {}^{18}\alpha \times \left(\delta^{18}O_f(O_2) + 1\right) - 1 \tag{3.5}$$

3.2 Measurement Setup

The measurement procedure has several steps including collecting air samples from different sites, CO_2 mole fraction measurement, CO_2 extraction from the air sample flasks, CO_2-O_2 isotope exchange reaction, CO_2-O_2 separation and determination of the $\Delta'^{17}O$, $\delta^{18}O$ and $\delta^{13}C$ values by using an isotope ratio mass spectrometer.

3.2.1 Sample collection

3.2.1.1 Sample collection sites

The air samples are collected from two different ecosystems.

The first sampling site is the Loobos Measurement Tower, which is a 24 meter high flux measurement tower located in an evergreen coniferous forest (evergreen coniferous forest ecosystem) near Kootwijk, The Netherlands. The tower is used for measuring the energy fluxes, radiation, turbulence, soil moisture, etc. For more information, see also https://ruisdael-observatory.nl/loobos/ and http://climatexchange.nl/sites/loobos/index.htm.

The second sampling site is the KNMI measuring mast Cabauw, which is a 213 meter high mast located in a grassland and river deposition area (grassland ecosystem) in Lopik near Utrecht, the Netherlands. The mast is used for meteorological and air composition measurements in the lower part of the atmosphere. For more information, see also https://www.knmi.nl/kennis-en-datacentrum/uitleg/meetmast-cabauw.

Figure 2. (a) Meteorological tower in Cabauw; (b) Loobos Measurement Tower; (c) The locations of the two observation sites; red: Cabauw; yellow: Loobos
(Source: https://www.icos-cp.eu/observations/national-networks/netherlands)

3.2.1.2 Sample collection methods

At Loobos Measurement Tower, air samples were taken at an altitude of 24.5 meters. At Cabauw, air samples were taken at an altitude of 200 meters. For each air sample, they were collected into two flasks of 1 litter and 2 litter volume, respectively. The air samples in 1L flasks were used to measure $\Delta'^{17}O$, $\delta^{18}O$, $\delta^{13}C$ values, and the 2L flasks were used for clumped isotope measurement (not discussed here).

Before collecting air samples, the flasks were cleaned by evacuating with low and then high vacuum pump, flushing with nitrogen gas for 1 hour, evacuating again in the oven with the temperature around 55℃. After that, the flasks were pressurized to around 1.5 bar by using compressed air with an atmospheric CO_2 content similar to that of the sampling air. When collecting air samples using these clean and pressurized flasks, the flasks were firstly flushed under the flow rate of 5 L/min for 10 minutes, then the flasks were filled with air sample to approximately 1.7 bar. A tube filled with magnesium perchlorate $Mg(ClO_4)_2$ was connected to the inlet of the flasks to be used as a dryer to reduce the moisture in the air before it went into the flasks to minimize potential isotope exchange with atmospheric moisture.

The samples were collected in the afternoon between 12:00 pm to 16:00 twice a month separately. The first air sample taken from Loobos started on 22 December, 2020 and the first air sample taken from Cabauw started on 22 December, 2020. The samples taken between December 2020 and May 2021 were adapted from part of an earlier master project from Melman, (2021). To acquire a complete seasonal cycle, we maintained sampling until May 2022.

3.2.2 CO_2 mole fraction measurement

Before CO_2 extraction, the CO_2 mole fraction from every air samples need to be measured by using a PICARRO model G2301 greenhouse gas concentration analyzer that precisely measures CO_2, CH_4 at parts-per-billion (ppb) and water (H_2O) vapor at parts-per-million (ppm). Around 50 ml of the air sample was taken out from the 1 litter flasks by using a syringe and then the air sample was injected into the PICARRO through the tube of inlet to measure the CO_2 mole fraction.

3.2.3 CO_2 Extraction

The first step to determine the isotope composition is extracting CO_2 from the air samples. A schematic of the extraction system is shown in Figure 3. The air sample is transferred from the flask into the CO_2 extraction system from the left side of the system. Then it is pumped through four cooling traps. The first 2 traps are cooled with a dry ice – ethanol slush, which is used to freeze the water out of the sample. The second two traps are cooled with liquid nitrogen (-196℃), which is used to freeze CO_2. The bulk air from the sample also passes through these traps but does not freeze, and is removed by a membrane vacuum pump. When all the gas has passed through the two traps, the CO_2 can be transferred to a sample vial which is submerged in liquid nitrogen by removing the liquid nitrogen dewar from trap 1.

After extracting the CO_2, the sample vial is taken to the IRMS to measure the $\delta^{13}C$ and $\delta^{18}O$ values of CO_2. After that, the CO_2 is collected back from the IRMS to the sample vial which is submerged in liquid nitrogen. Then the CO_2 sample is taken to next procedure for isotope exchange reaction.

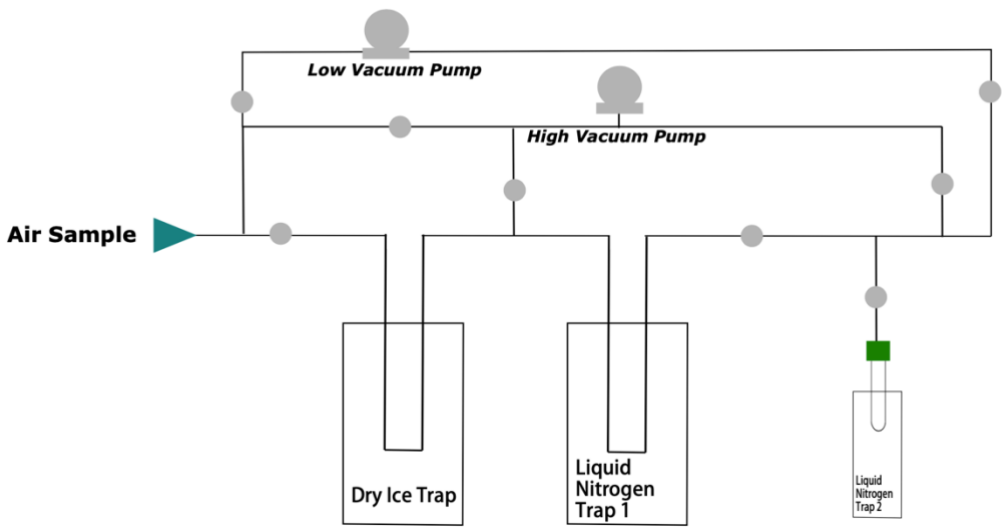

Figure 3. Schematic of CO_2 extraction system.

3.2.4 CO_2-O_2 isotope exchange reaction

The schematic of the CO_2-O_2 isotope exchange and CO_2-O_2 separation system is shown in Figure 4. The extracted CO_2 sample is first transferred into the exchange system and expanded into the quartz reactor. The CO_2 is frozen and trapped in the reactor under valve 26. The cooling of the reactor is realized by slowly passing liquid nitrogen from a liquid nitrogen microdosing system (Norhof 900 series LN_2 cooling system, Ede, The Netherlands) through a horizontal tube that goes through the reactor. After that, an approximately equal amount of O_2 with known initial isotope composition is also transferred to the exchange system from a O_2 cylinder. The O_2 is expanded into the quartz reactor. Then the CO_2 is released from the horizontal tube to mix with O_2 by closing the LN_2 microdosing system. The quartz reactor contains a platinum catalyst of approximately 0.2 g at the bottom and the bottom part of the reactor is inserted into a tube oven where it is heated to 750 °C. The CO_2-O_2 isotope exchange is performed for 2 hours.

3.2.5 CO_2-O_2 separation

After isotope exchange is complete, the double U trap next to the quartz reactor (trap 3) is cooled down by liquid nitrogen for 5 minutes in order to make sure the temperature becomes low enough. The reactor is then opened and the gas will go through the U trap where CO_2 is cryogenically collected while O_2 passes the trap and is collected in a sample vial containing 3 molecular sieve 5 Å pellets. The molecular sieve is used to absorb O_2 into its pores. The sample vial is submerged in liquid nitrogen dewar 4 for 10 minutes to make sure O_2 is completely absorbed. After that, the sample vial is closed manually and then submerged in water to warm up in order to release the O_2 molecules from the molecular sieve.

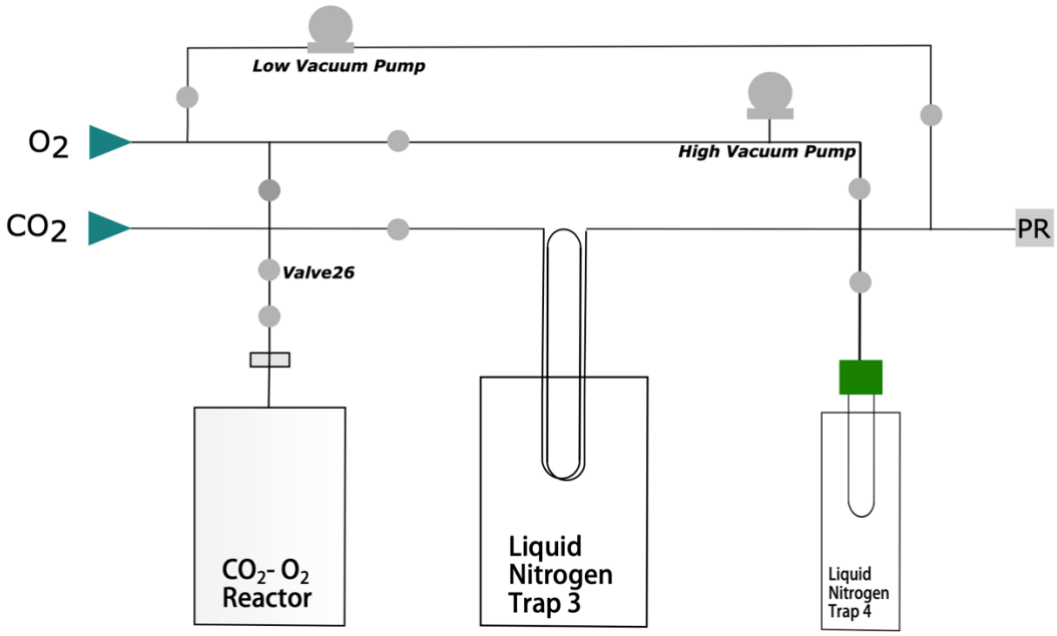

Figure 4. Schematic of the CO_2-O_2 isotope exchange reaction and CO_2-O_2 separation system. (Valves: Grey dots; Pressure gauge: PR)

3.2.6 Determination of isotope ratios using Isotope ratio mass spectrometer

After isotope exchange, the O_2 sample is taken to a Thermo Scientific isotope ratio mass spectrometer (IRMS) to measure the isotopic composition of O_2 after exchange. The O_2 sample we need to measure is filled into the left bellow and the reference O_2 gas is filled into the right bellow of the dual inlet system with equal amounts.

The isotope ratio mass spectrometer operates by separating the ionised molecules of interest in a magnetic field according to their mass-to-charge ratio (m/z). Beams with lighter ions (from the isotopically lighter molecules) bend at a smaller radius than beams with heavier ions (from the isotopically heavier molecules). The current of each ion beam is then measured by using a 'Faraday cup'. The ratio of the current measured by each cup is compared to the ratio generated by the reference gas, and then delta values can be produced.

The reference gas in the bellow is pumped out and reloaded for each new measurement both for CO_2 and O_2 since the reference gas in the bellow may be gradually enriched in heavy isotopes, as the lighter isotopes will preferentially leak out from the capillary connected to the bellow according to Yan et al., 2022.

3.3 Calibration of the system

3.3.1 Zero Enrichment

In order to establish the accuracy and stability of the mass spectrometer and the precision of the output, we carried out a zero enrichment experiment every day before the sample measurement. To do this, we filled both bellows of the dual inlet system with same amount of reference gas (GAA_O_2 for oxygen and Carl_CO_2 for CO_2 measurement) with known isotope composition.

In principle, the output of $\delta^{17}O$, $\delta^{18}O$ and $\Delta'^{17}O$ should be equal to 0 because the two bellows contain same gas with same isotope composition. However, the results always showed some bias. These values were either slightly larger or smaller than 0. This bias, or deviation between the two bellows needs to be taken into account. Therefore, a correction was performed based on these experiments to remove the zero enrichment bias for each experiment.

Apart from that, there might be some outlier data points that represent bad results with large deviations. In this case, we need to repeat the zero enrichment experiments to check the stability again. If the results still go wrong after repeating the experiment several times, then we need to check whether the machine is malfunctioning. Meanwhile, these outlier data points are removed when performing a correction.

3.3.2 N_2O Correction for CO_2

The process of extracting CO_2 from air samples requires separation from air by using liquid nitrogen, however, N_2O is also condensed along with CO_2 at the same time. Different isotopic species of N_2O and CO_2 have almost the same molecular masses (44, 45, 46), therefore the present of N_2O would cause deviation when analyzing the isotopic composition of CO_2 by using the isotope ratio mass spectrometer. (Ghosh et al., 2004) In order to avoid the interference of N_2O on $\delta^{13}C$ and $\delta^{18}O$ measurements of extracted CO_2, a correction must be performed for the raw $\delta^{13}C$ and $\delta^{18}O$ values after analyzing by isotope ratio mass spectrometer. (Assonov et al., 2006) When CO_2 is extracted from atmospheric air or soil gas samples, the values of the N_2O correction are +0.225‰ for $\delta^{13}C$ and +0.325‰ for $\delta^{18}O$ values according to Gorczyca et al., (2004). And according to Hofmann et al., 2017, the values of the N_2O correction are $+0.22‰ \pm 0.03‰$ for $\delta^{13}C$ and $+0.29‰ \pm 0.03‰$ for $\delta^{18}O$ for ambient air CO_2. In this study, we corrected for N_2O using $\delta^{13}C$ values of +0.2‰ and $\delta^{18}O$ values of +0.3‰.

4 Part 1: Investigation of the stability and potential analytical artifacts of CO_2 - O_2 isotope exchange system

We need to ensure the stability and accuracy of the CO_2 - O_2 isotope exchange system. However, some potential influential factors such as reaction time, reaction pressure, reaction temperature and temperature gradients in the reactor may affect the exchange reaction and result in analytical biases, which would affect the $\Delta'^{17}O$ quantification. Therefore, in part 1 of this thesis, several experiments were carried out to investigate important parameters of the system.

4.1 Investigation of equilibrium reaction times for CO_2-O_2 exchange reactions at different reactor pressures

In order to investigate the equilibrium reaction times for CO_2-O_2 isotope exchange reaction and see if it will depend on different reactor pressures, several experiments are carried out by varying the reaction time from 5 minutes to 120 minutes as well as adjusting the reactor pressures to 60 mbar, 84 mbar and 120 mbar by putting different amount of CO_2-O_2 into the reactor. The experiments for each variable were repeated for 2 ~ 3 times to ensure experiment reproducibility and reduce experimental result inaccuracy.

Figure 5 a, b show the temporal evolution of $\delta^{18}O$ and $\delta^{17}O$ values during the CO_2-O_2 isotope exchange reaction under 3 different reactor pressures respectively. When the reaction time is longer than around 30 mins, $\delta^{18}O$ (CO_2) and $\delta^{18}O$ (O_2) approximately reach the equilibrium state. In our experiments, we still kept the reaction time to 2h to be consistent with previous experiments.

Fig 5a shows that for larger reactor pressures, it takes relatively longer time to reach the equilibrium. There is a small difference between the final isotopic values of $\delta^{18}O$ (CO_2) and $\delta^{18}O$ (O_2) after reaching the equilibrium state. This can be explained by the thermodynamic properties that CO_2 and O_2 will not reach perfectly identical isotopic composition. The difference between them is defined as fractionation factors ${}^{18}\alpha$, according to the equation 3.4. ${}^{18}\alpha$ becomes approximately stable after 30 minutes reaction time. And the final values of ${}^{18}\alpha$ only have very slightly differences under different reaction pressures. Table 2 shows $\delta^{18}O$ (O_2), $\delta^{18}O$ (CO_2) and their standard error for each experiment. The standard errors range from 0.001 to 0.002 for $\delta^{18}O$ (O_2) and ranging from 0.002 to 0.005 for $\delta^{18}O$ (CO_2), which is much smaller than the fractionation factors after complete equilibrium. Therefore, the effect caused by the experiment can be neglected.

Reactor Pressure	Reaction Time [mins]	O_2		CO_2	
		$\delta^{18}O$[‰]	Standard Error	$\delta^{18}O$[‰]	Standard Error
60 mbar	5	21.002	0.002	23.127	0.003
	7	21.468	0.001	22.683	0.004
	10	21.732	0.001	22.443	0.003
	10	21.727	0.001	22.495	0.003
	10	21.743	0.001	22.413	0.004
	25	21.865	0.001	22.377	0.003
	30	21.835	0.001	22.316	0.004
	60	21.817	0.001	22.292	0.004
	90	21.843	0.001	22.288	0.004
	120	21.877	0.002	22.334	0.004
84 mbar	5	20.694	0.001	23.432	0.003
	7	21.249	0.002	22.905	0.003
	10	21.643	0.001	22.513	0.004
	25	21.837	0.001	22.304	0.003
	30	21.905	0.001	22.287	0.003
	60	21.851	0.001	22.289	0.005
	90	21.853	0.001	22.293	0.005
	30	21.848	0.002	22.295	0.004
	100	21.837	0.002	22.317	0.003
	120	21.879	0.001	22.290	0.003
120 mbar	5	20.241	0.001	23.879	0.003
	7	20.950	0.001	23.191	0.003
	10	21.362	0.001	22.769	0.002
	25	21.824	0.001	22.315	0.003
	30	21.845	0.002	22.302	0.002
	60	21.787	0.001	22.294	0.003
	90	21.844	0.001	22.302	0.003
	120	21.911	0.001	22.281	0.002

Table 2. $\delta^{18}O$ (O_2) and $\delta^{18}O$ (CO_2) for CO_2-O_2 isotopic exchange experiments at reaction temperature of 750 ◦C and reaction pressures of 60 mbar, 84 mbar and 120 mbar for different reaction time.

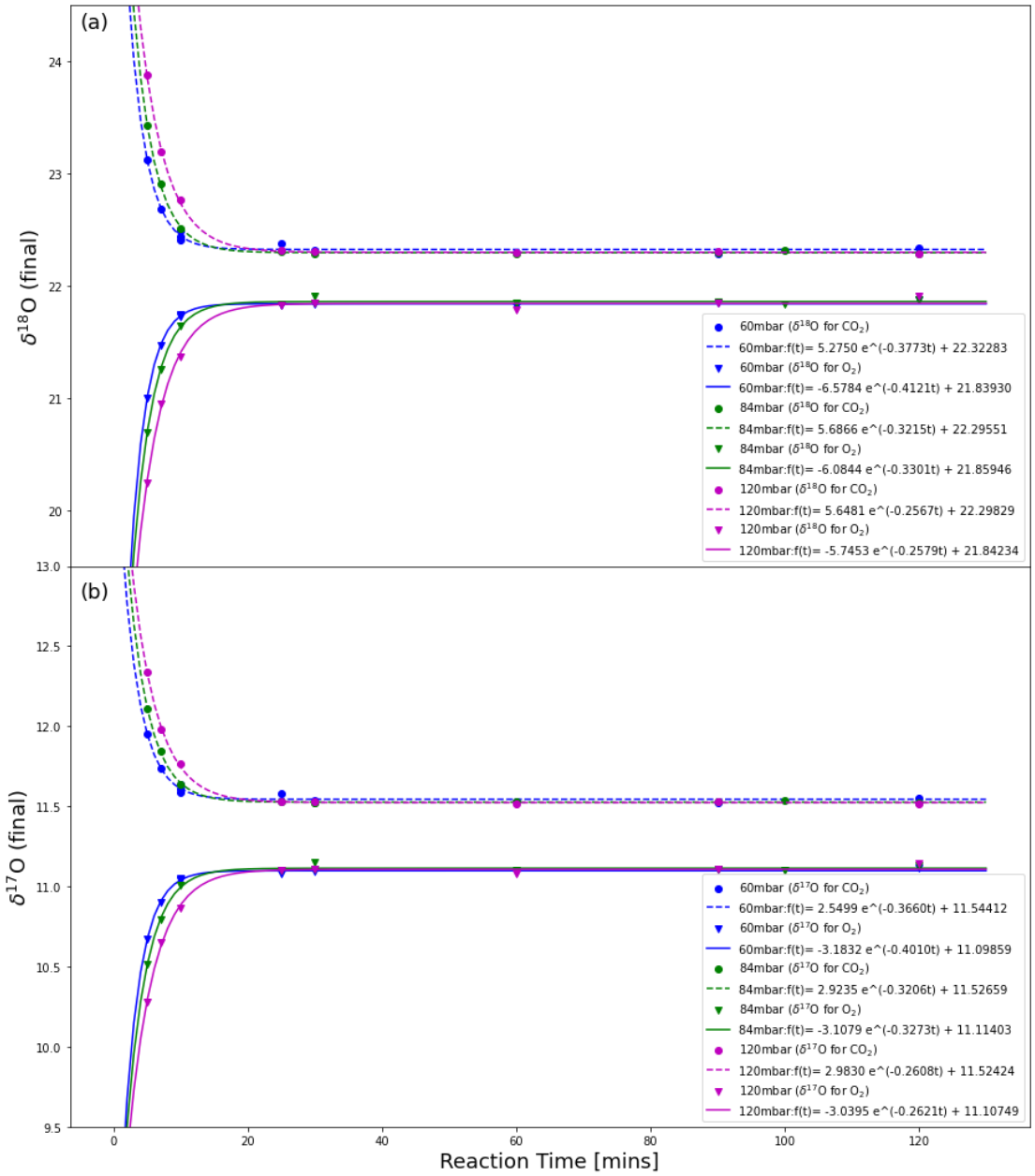

Figure 5. Temporal evolution of a) $\delta^{18}O$ (CO_2) and $\delta^{18}O$ (O_2) and b) $\delta^{17}O$ (CO_2) and $\delta^{17}O$ (O_2) during the CO_2-O_2 isotope exchange reaction for reaction pressures of 60 mbar, 84mbar and 120mbar.

4.2 Stability of CO_2-O_2 isotope exchange system and determination of the fractionation factors

Before measuring the air samples, a large number of measurements were carried out to i) determine the reproducibility of the CO_2 -O_2 exchange system, and ii) determine the O_2-CO_2 fractionation factor in the reactor, before air samples could be measured. In these experiments we put equal amounts of O_2 and CO_2 mixture with known initial

isotope composition into the quartz reactor (reactor pressure = 60 mbar) to exchange isotopes at 750 ℃ until they reach equilibrium. After the experiments, $\delta^{17}O$, $\delta^{18}O$, ${}^{17}\alpha$ and ${}^{18}\alpha$ values were evaluated and compared with previous studies to make sure the isotope exchange system and results are reproducibility.

Table 3 shows the results of 15 repetitions the experiment, the averages, standard deviations and standard error are given. From these results we determined the average fractionation factors to be ${}^{17}\alpha = 1.000488 \pm 5.334 \times 10^{-6}(\mathrm{SE})$ and ${}^{18}\alpha = 1.000564 \pm 9.688\mathrm{E} \times 10^{-6}(\mathrm{SE})$ at reaction temperature of 750 ˚C.

Exp No.	${}^{17}\alpha$	${}^{18}\alpha$
1	1.000507	1.000628
2	1.000465	1.000530
3	1.000505	1.000580
4	1.000469	1.000569
5	1.000471	1.000538
6	1.000498	1.000583
7	1.000517	1.000619
8	1.000527	1.000618
9	1.000478	1.000525
10	1.000478	1.000560
11	1.000495	1.000557
12	1.000455	1.000499
13	1.000479	1.000532
14	1.000477	1.000548
15	1.000500	1.000573
Average	1.000488	1.000564
Standard deviation	0.000021	0.000038
Standard error	5.334×10^{-6}	9.688×10^{-6}

Table 3. The fractionation factors for CO_2-O_2 isotopic exchange experiments at reaction temperature of 750 ˚C and reaction pressure of 60 mbar for 2 hours.

4.3 Investigation of potential isotope exchange with molecular sieve, silica gel and the quartz reactor.

In order to investigate whether any isotope effect will occur when only CO_2 or O_2 pass through the quartz reactor at high temperature, we carried out two experiments for CO_2 and O_2 with known initial isotope composition respectively. The initial isotope composition for O_2 used here is $\delta^{18}O_{ref}$ = 14.095‰, $\delta^{17}O_{ref}$ = 7.044‰. For the first experiment, CO_2 and O_2 were trapped in the quartz reactor at p = 30 mbar, T = 750℃.

After being trapped in the reactor for 2 hours, the CO_2 or O_2 were collected into the sample vial and then taken to the mass spectrometer to measure the changes in the isotopic composition. For the second experiment, equal amounts of CO_2 and O_2 were collected directly to the sample vial without going through and being trapped in the quartz reactor for 2 hours. The $\delta^{17}O$, $\delta^{18}O$ values from these experiments were then compared with the normal procedure.

Molecular sieve has a defined structure with uniform crystalline pores , while silica gel has an amorphous structure with many irregular pores, both of them can help to absorb O_2 onto their pores. The interaction of O_2 with molecular sieve pellets and silica gel pellets can lead to different fractionation due to their potential isotope exchange. We carried out an experiment in order to investigate which pellet causes less fractionation and is more stable for collecting O_2. For this experiment, O_2 was trapped in the quartz reactor at p = 30 mbar, T = 750℃ for 2 hours. After that, O2 was collected into the sample vials contain of molecular sieve or silica gel respectively. 11 replicate experiments were performed for molecular sieve and 9 replicate experiments were performed for silica gel. The $\delta^{17}O$, $\delta^{18}O$ and $\Delta'^{17}O$ values from these experiments were then compared with each other.

$d^{17}O$ and $d^{18}O$ are defined as the deviation of $\delta^{17}O$ and $\delta^{18}O$ before and after the experiments, which can be calculated by $d^{17}O = \delta^{17}O_{final} - \delta^{17}O_{ref}$ and $d^{18}O = \delta^{18}O_{final} - \delta^{18}O_{ref}$ respectively. ($\delta^{17}O_{ref}$ represents the initial values of $\delta^{17}O$ and $\delta^{17}O_{final}$ represents the final values of $\delta^{17}O$) For these experiments, $d^{17}O$ and $d^{18}O$ values should be equal to 0 in principle, because the same O_2 gas with same initial isotope composition were used for all experiments. However, the results showed that there is the offset between the isotopic composition.

Figure 6a, 6b, 6c show the dependency of $d^{17}O$, $d^{18}O$ and $\Delta'^{17}O$ after the interaction of the oxygen with molecular sieve, silica gel with and without the heating step in the quartz reactor, and zero enrichment for O_2 respectively. The green and red points represent the dependency of $d^{17}O$, $d^{18}O$ and $\Delta'^{17}O$ with heating step in contact with molecular sieve and silica gel, respectively. The blue points represent the results from without heating step and without contact with molecular sieve or silica gel . The purple point represents the result from zero enrichment.

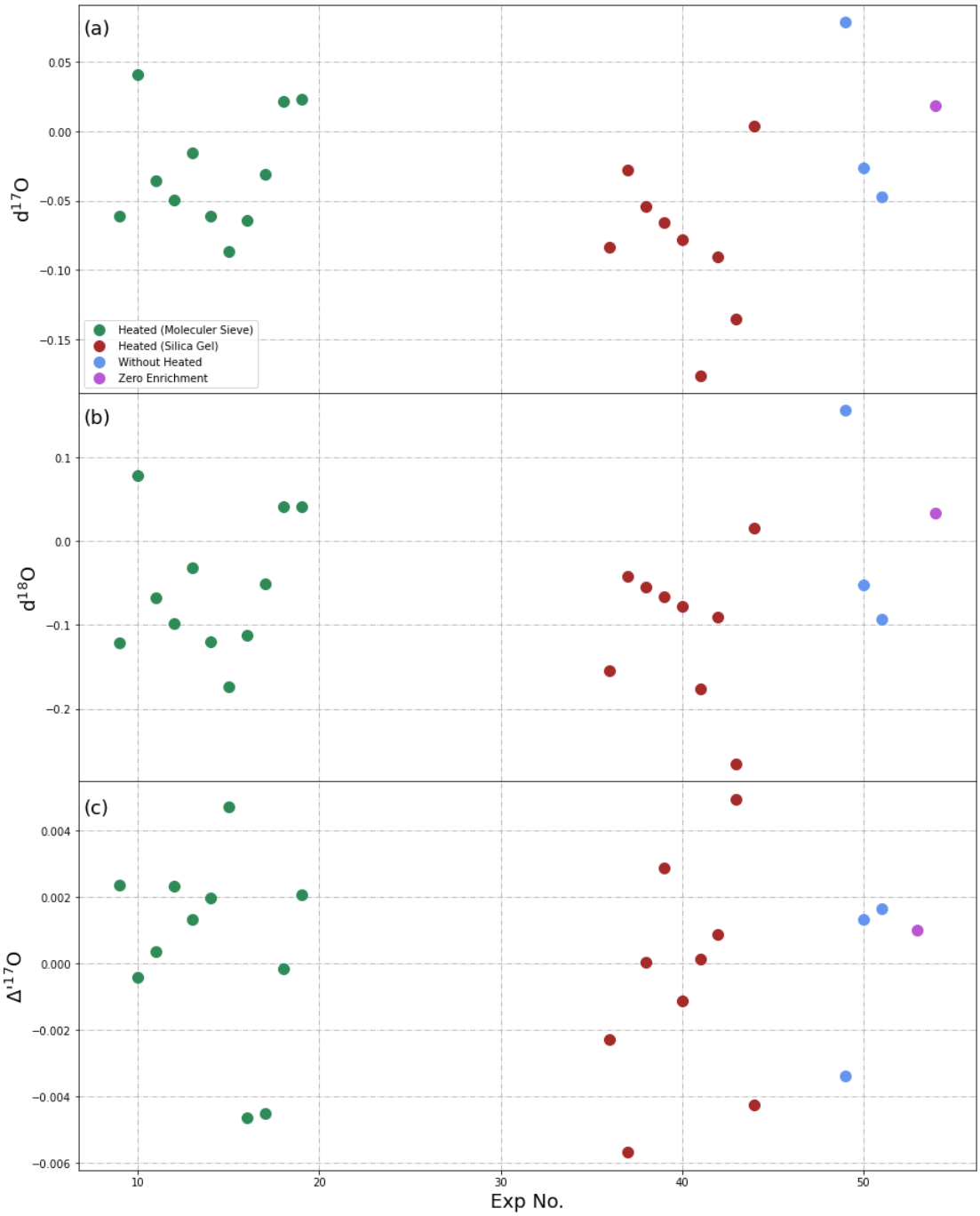

Figure 6. Dependency of a) $d^{17}O$ ($\delta^{17}O_{final}-\delta^{17}O_{ref}$) , b) $d^{18}O$ ($\delta^{18}O_{final}-\delta^{18}O_{ref}$), c) $\Delta'^{17}O$ on contact with molecular sieve and silica gel, and with and without the heating step in the quartz reactor, and zero enrichment for O_2.

		$d^{17}O$[‰]	$d^{18}O$[‰]	$\Delta'^{17}O$[‰]
Molecular Sieve	Mean	-0.026	-0.049	0.0002
	Std. dev.	0.042	0.081	0.003
Silica Gel	Mean	-0.050	-0.092	-0.0011
	Std. dev.	0.042	0.084	0.004
Unheated	Mean	-0.037	-0.072	-0.0001
	Std. dev.	0.015	0.029	0.003
Zero Enrichment		0.019	0.034	0.001

Table 4. Dependency of $d^{17}O$, $d^{18}O$ and $\Delta'^{17}O$ on contact with molecular sieve, silica gel with and without the heating step in the quartz reactor, and zero enrichment for O_2.

The results shown in table 4 indicate that the experiments where O_2 interacted with molecular sieve have less isotope bias and are more stable compared to those using silica gel. Therefore for the measurement for air samples, a molecular sieve was selected for collecting O_2. As the bias between the isotopic composition of O_2 due to the interaction of the O_2 with the molecular sieve were determined in these experiments, a correction was performed for the values of $\delta^{17}O$, $\delta^{18}O$, $\Delta'^{17}O$ for O_2 that needed to be measured after exchange reaction.

As shown above, there is still bias between the isotope composition of O_2 for unheated experiments and without having contact with molecular sieve compared to zero enrichment. One possible reason for this bias could be that the GAA_O_2 cylinder was filled in 28th November 2018, the original values of isotopic compositions were defined in 2018, the isotopic compositions may have undergone some changes in the cylinder over time. The bias for $\delta^{17}O(O_2)$ and $\delta^{18}O(O_2)$ shown in table 5 are determined by unheated experiments and zero enrichment. Therefore, the new definition for isotope compositions including $\delta^{17}O$, $\delta^{18}O$ for reference GAA_O_2 cylinder are corrected as $\delta^{17}O(O_2) = 7.022‰ \pm 0.015‰(SD)$ and $\delta^{18}O(O_2) = 14.053‰ \pm 0.029‰(SD)$. Moreover, the results indicate that there are significant isotope effects on $\delta^{17}O$ and $\delta^{18}O$, but the effects on $\Delta'^{17}O$ are insignificant.

	$\delta^{17}O(O_2)$	$\delta^{18}O(O_2)$
Original values	7.044‰	14.095‰
Bias	-0.021‰	-0.041‰
New values	$7.022‰ \pm 0.015‰$	$14.053‰ \pm 0.029‰$

Table 5. The original values and the newly defined values of isotope composition of O_2 for reference GAA_O_2 cylinder.

According to the heated and unheated experiments for CO_2, there is also a deviation for isotope composition from unheated experiments. Therefore, the new definition for isotope compositions for the reference CO_2 cylinder are defined as $\delta^{17}O(CO_2)$ = 15.542‰ $\pm$ 0.005‰ and $\delta^{18}O(CO_2)$ = 29.959‰ $\pm$ 0.005‰.

4.4 Effect of temperature gradients in the reactor on the fractionation of CO_2 - O_2 isotope exchange reaction

According to figure 7 (from Adnew et. al., 2021), $\alpha^{17}(CO_2/O_2)$ and $\alpha^{18}(CO_2/O_2)$ have a clear dependency on the quartz reactor temperature both from experiments and theoretical calculations for CO_2 - O_2 isotope exchange reaction. When the reactor temperatures are higher, the equilibrium fractionation factors between CO_2 and O_2 are smaller. The theoretical calculations for α approach unity at higher temperature. However, the fractionation constants from the experiment are always lower than the corresponding theoretically calculated values and slightly below unity at higher temperature.

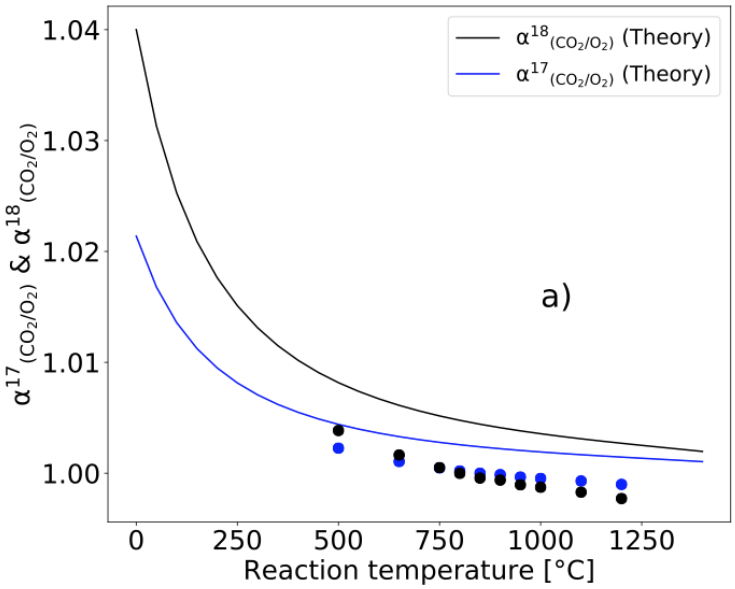

Figure 7. Dependency of $\alpha^{17}(CO_2/O_2)$ and $\alpha^{18}(CO_2/O_2)$ on the temperature and comparison with the theoretical calculations (Adnew et. al., 2022). The blue and black dots represent the results from experiments. The blue and black solid lines are the results from theoretical calculations.

Figure 8 shows the sketch of the quartz reactor that is used for CO_2-O_2 exchange. The CO_2-O_2 mixture is trapped in the quartz reactor below the valve 26 to let CO_2 and O_2 exchange isotopes at high temperature (750 ℃). However, only part of the reactor is inserted into the oven, and some gas is in the cold zone above the oven. The temperature near the horizontal glass tube of liquid nitrogen inlet is between 90 ~99 ℃, which is much lower than the reactor temperature in the oven near heated platinum. Therefore, there is a large temperature gradient between valve 26 and the oven. This could lead to an isotope affect associated with thermal diffusion of isotopes between the hot and cold zones.

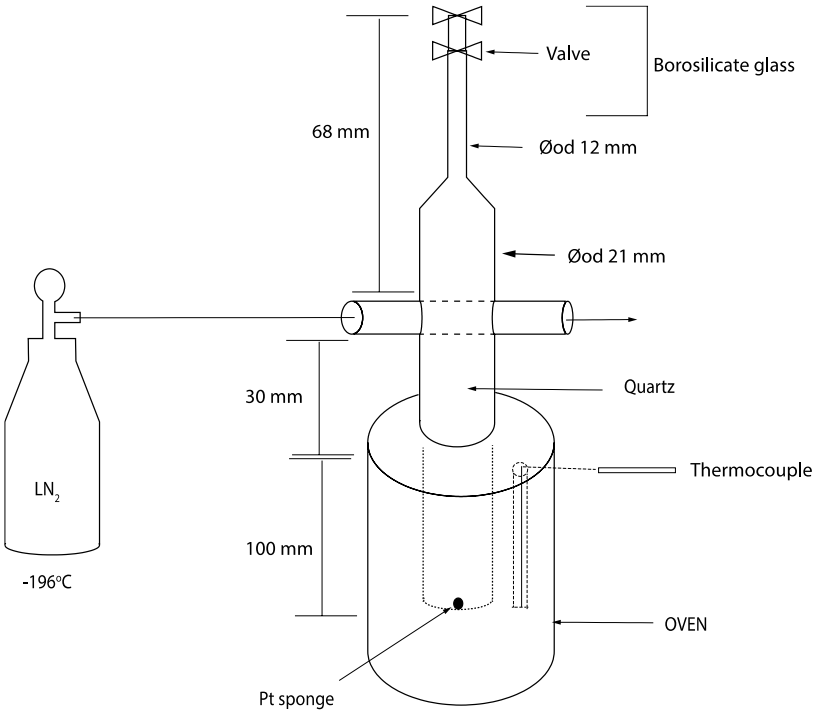

Figure 8. Geometry and dimensions of the CO_2-O_2 exchange reactor used by Adnew et al. (2019).

In order to investigate whether the difference between the theoretical and experimental results is due to the thermal diffusion in the reactor, the temperature gradients in the reactor were varied by adjusting the temperature near the horizontal tube that is used to cool the reactor with liquid nitrogen. When the temperature near the horizontal tube was lower, the temperature gradient will become larger. The temperature near the horizontal tube was changed by letting different amounts of cold nitrogen flow through this tube by adjusting the liquid nitrogen microdosing system.

In this experiment, equal amounts of CO_2 and O_2 with known initial isotopic composition were used for the CO_2-O_2 isotope exchange reaction. Firstly, the mixture of CO_2 and O_2 was trapped in the reactor to exchange isotopes at constant reactor temperature equal to 750℃ and at constant reactor pressure equal to 60 mbar for 2 hours. The temperature near the horizontal tube was adjusted to 90℃, 0℃, -40℃, -60℃, -80℃ respectively, therefore the temperature gradients ranged from 660℃ to 830℃. Secondly, the reactor temperature was set to 1000℃ with constant reactor pressure equal to 60 mbar for 2 hours. The temperature near the horizontal tube was adjusted to 150℃, 60℃, 0℃, -20℃, -40℃, -80℃ respectively, so the temperature gradients range from 850℃ to 1080℃. Note that the reactor pressure was calculated assuming that the temperature near the horizontal tube and the reactor are room temperature(~25℃) for

these experiments. For each temperature gradient, the experiments were performed several times to confirm that the results are reliable.

Figure 9 shows the dependency of $\alpha^{18}(CO_2/O_2)$ on the temperature gradients, ranging from 660℃ to 1080℃. As expected, the fractionation value decreases with increasing temperature gradients. At reactor temperature of 750℃, which has smaller temperature gradients, the fractionation values are higher than the values when reactor temperature equals to 1080℃ (note the different y axis scales). Larger thermal diffusion (larger temperature gradients) will lead to smaller fractionation both for reactor temperature of 750℃ and 1000℃.

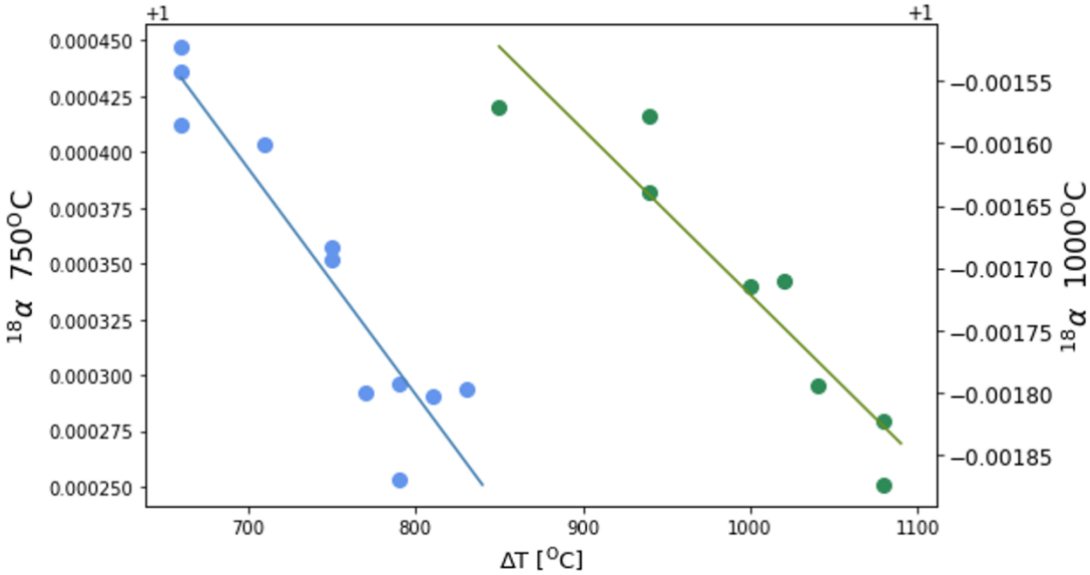

Figure 9. Dependency of $^{18}\alpha(CO_2/O_2)$ on different temperature gradients between 660 ℃ and 830 ℃ under reactor temperature equal to 750 ℃ (blue points) and temperature gradients between 850℃ and 1080℃ under reactor temperature equal to 1000℃ (green points) respectively. Linear fit for reactor temperature of 750℃ (blue line): $^{18}\alpha = -1.013 \times 10^{-6}\,\Delta T + 1.001$; Linear fit for reactor temperature of 1000℃ (green line): $^{18}\alpha = -1.324 \times 10^{-6}\,\Delta T + 0.996$.

4.5 Stability of the IRMS: Temporal evolutions of zero enrichment for CO_2 and O_2 for the mass spectrometers

To investigate the experimental precision of the IRMS and ensure the system stability for each measurement, the zero enrichment experiments were performed by putting equal amount of same reference gas in the two bellows almost every day before the experiments. There are two mass spectrometers being used for CO_2 and O_2 measurement respectively, namely IRMS A and IRMS B. During the time period from

November 2021 to June 2022, the results for the zero enrichment for IRMS A are not always stable.

The figures 10 a, b below show the results of $\delta^{18}O$ and $\delta^{13}C$ for CO_2 zero enrichment experiments by using IRMS A. The large deviations around 29th March 2022 occurred when the ion source was changed and the inlet capillary of IRMS A was broken. After the ion source and the capillary were replaced, the results of the experiments changed sign reversed (from negative values to positive values). In the period before the capillary replacement, the average zero enrichments are $\delta^{18}O = -0.050‰ \pm 0.021‰$ and $\delta^{13}C = -0.025‰ \pm 0.009‰$ from November 2021 to March 2022. After the capillary replacement, the average zero enrichments are $\delta^{18}O = 0.030‰ \pm 0.010‰$ and $\delta^{13}C = 0.019‰ \pm 0.007‰$.

Almost all the experiments after the replacement of the capillary were performed for around 200 acquisitions, to make sure the values are reproducible. For the first few acquisitions for each experiment, the signal intensity was unstable fluctuating over a large range, which led to inconsistent and scattered results. There are several potential reasons for this scatter.

1) When the gas flows through the narrow capillary from the bellow, the lighter isotopes may preferentially leaked out.
2) When the gas flows through the narrow capillary from the bellow, very small amounts of other gases may leak into the system from the outside.
3) There was still an oxygen reservoir in the capillary or other part of the inlet system that has not been completely cleaned out, so there may be isotope exchange.

There could be many other factors that lead to these deviations and we are unable to identify what caused such deviations.

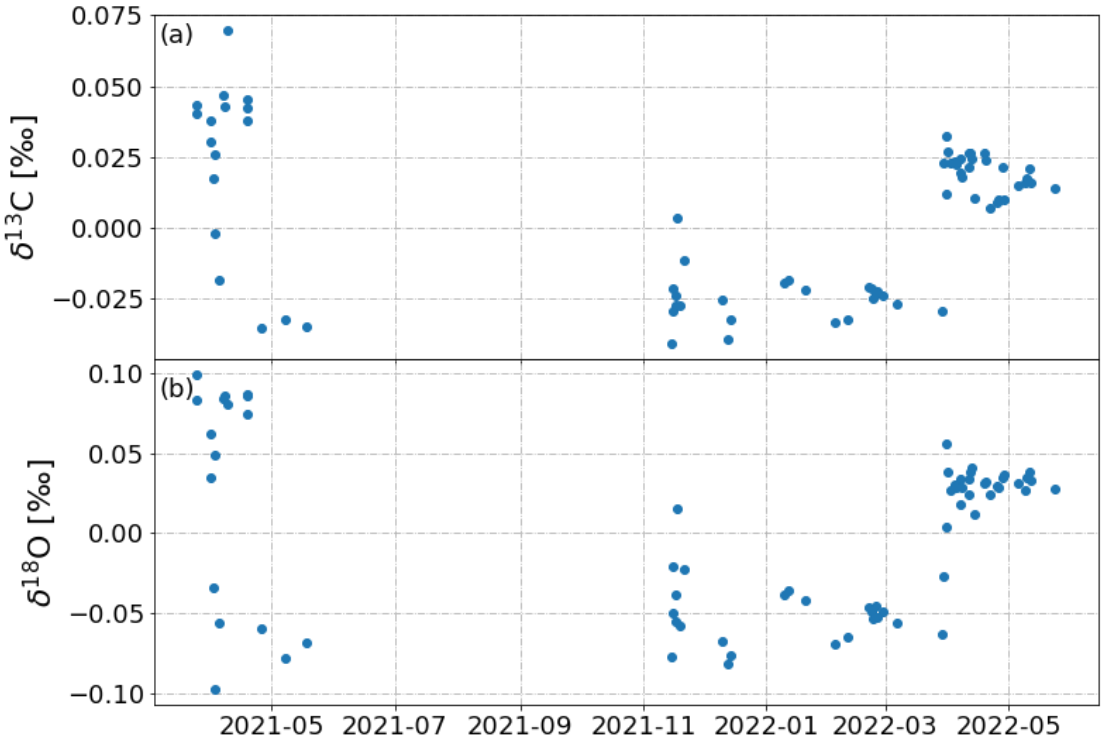

Figure 10: Temporal evolution of the results of a) $\delta^{13}C$ [‰] and b) $\delta^{18}O$ [‰] for CO_2 zero enrichment of the IRMS from November 2021 to June 2022.

The figure 11 below shows the results of $\delta^{17}O$, $\delta^{18}O$ and $\Delta'^{17}O$ for O_2 zero enrichment experiments by using IRMS B from August 2021 to June 2022. The averages of the results from the zero enrichment experiments are $\delta^{17}O = 0.0208‰ \pm 0.0079‰$, $\delta^{18}O = 0.0398‰ \pm 0.149‰$ and $\Delta'^{17}O = 0.0002‰ \pm 0.0038‰$ after removing the outliers (red point in figure 11).

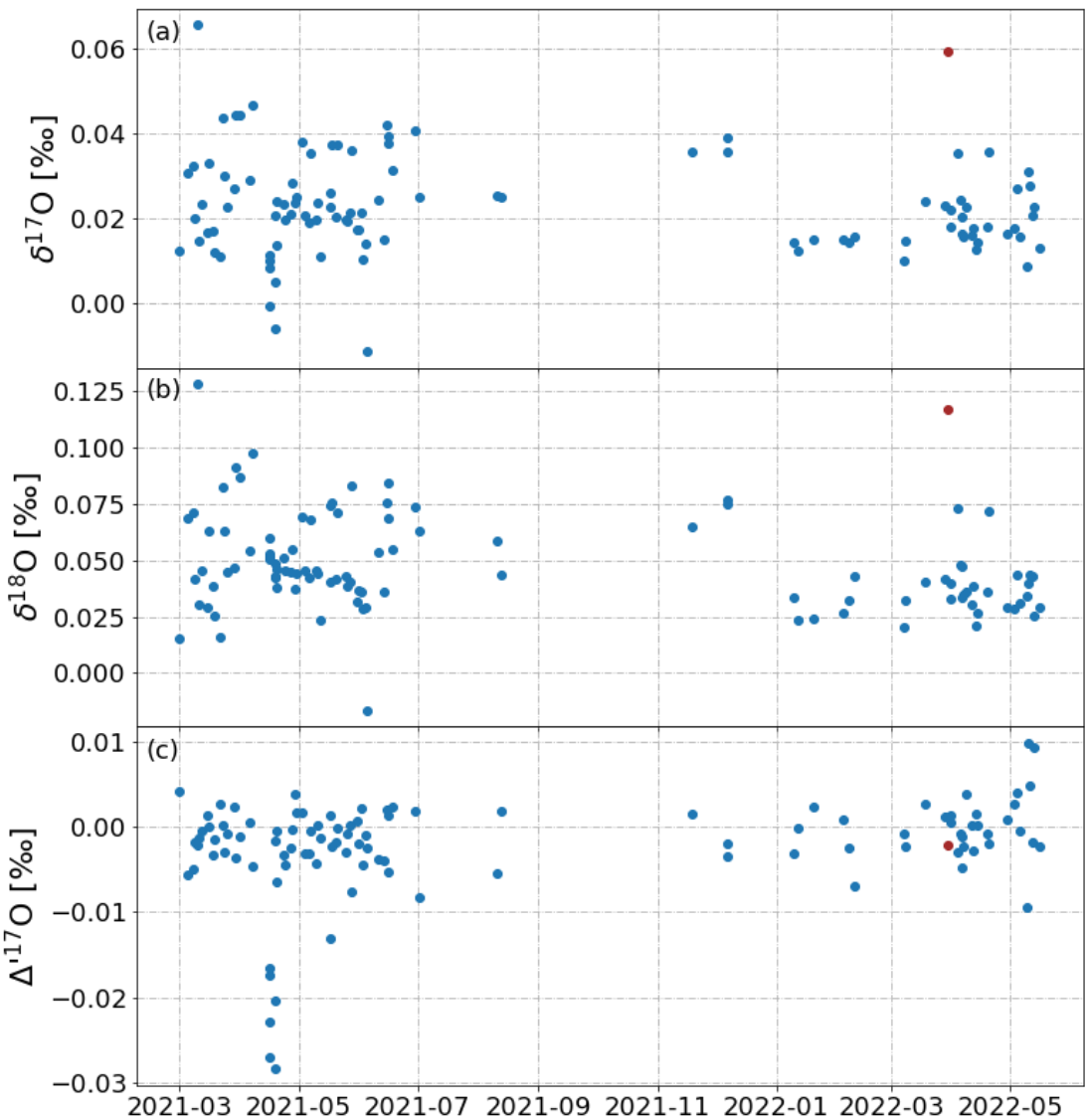

Figure 11: Temporal evolution of the results of a) δ^{17}O [‰], b) δ^{18}O [‰] and c) Δ'^{17}O [‰] for O_2 zero enrichment from March 2021 to June 2022.

5 Part 2: Investigation of the seasonal variation in $\delta^{13}C$, $\delta^{18}O$ and $\Delta'^{17}O$ value of troposphere CO_2

In the second part of the thesis, the temporal evolution of $\delta^{13}C$, $\delta^{18}O$ and $\Delta'^{17}O$ values were measured by using the CO_2-O_2 isotope exchange system for air samples collected from Cabauw and Loobos to investigate the seasonal variation of $\delta^{13}C$, $\delta^{18}O$ and $\Delta'^{17}O$ values of tropospheric CO_2.

5.1 Experimental Results

Table 6 and Table 7 below show the time series of CO_2 mole fraction, $\delta^{13}C$, $\delta^{18}O$ and $\Delta'^{17}O$ with standard error for two measurement locations Cabauw and Loobos respectively. Data from July to August of 2021 are not available since there was no sample collection. Figure 12 below shows the overview of temporal evolution of $\delta^{13}C$ values [‰], $\delta^{18}O$ values [‰] and $\Delta'^{17}O$ values [‰] from December 2020 to April 2022 from Cabauw and Loobos. The outliers are marked by orange points or yellow points.

There are four abnormal results from the end of June to the beginning of October for Cabauw, especially for the $\delta^{18}O$ values that scatter over a large range. This period is marked by grey shading. The outliers for $\delta^{18}O$ values are removed in figure 11 (c) in order to have a better overview of the seasonal pattern. When evaluating the results, these four outlier points and few other measurements that are suspected to be biased (also marked by grey shading) are removed.

The CO_2 - O_2 exchange system became unstable and the platinum catalyst was broken and replaced after a few experiments of the samples. The heater for the CO_2 - O_2 exchange reactor was broken. Therefore, the measurements were interrupted and the results from Loobos are incomplete. But we still obtain the results for $\delta^{18}O$, $\delta^{13}C$ values sampled in Loobos from December 2020 to December 2021 and several results for $\Delta'^{17}O$ values from December 2020 to September 2021.

5.1.1 CO_2 mole fraction, $\delta^{13}C$, $\delta^{18}O$ and $\Delta'^{17}O$ values in Cabauw

As expected, the CO_2 mole fraction values show a downward trend from March to June, and then reached a minimum in summer, with a range from 411 ppm in June to 428 ppm in February, an average of 421.5 ppm, and with a seasonal amplitude of around 17 ppm. Measurements for $\delta^{13}C$ values show an increasing trend when approaching summer and a decreasing trend toward winter, ranging from -9.9‰ on March 2022 to -8.8‰ on June 2021. The $\delta^{13}C$ values in Cabauw have a seasonal amplitude of around 1.1‰ and an average of -9.2‰. The $\delta^{18}O$ values in Cabauw ranged from 39.9‰ in

December 2021 to 41.8‰ in June 2021, with a very clear seasonal cycle of relatively high values during summer and low values during winter. The $\delta^{18}O$ values in Cabauw have a seasonal amplitude of around 1.9‰ and an average of 40.8‰.

The results of $\Delta'^{17}O$ values in Cabauw range from -0.184‰$\pm$0.004‰(SE) in October to -0.264‰$\pm$0.012‰(SE) in January, with a seasonal amplitude of around 0.08‰ and an average of $\Delta^{17}O$ values equal to -0.221‰$\pm$0.006‰(SE). There is a slight upward trend from December 2020 to June 2021, which was reported by Melman, (2021) but the results are scattered. Focusing on the period from October 2021 to April 2022, the new measurements reported in this thesis, the results of $\Delta'^{17}O$ values show more scatter, without clear upward or downward patterns.

5.1.2 CO_2 mole fraction, $\delta^{18}O$, $\delta^{13}C$ and $\Delta'^{17}O$ values in Loobos

The CO_2 mole fraction values indicate a distinct downward trend when approaching summer and a upward trend towards winter, ranging from 399.3 ppm in August to 429.5 ppm in October, with a seasonal variation of around 30 ppm and an average of 419.3 ppm. The $\delta^{13}C$ values varied between -8.2‰ and -9.5‰, with a seasonal variation of 1.3‰ and an average of -9.0‰. The seasonal cycle of $\delta^{13}C$ show higher values during summer and lower values during winter. The $\delta^{18}O$ values varied from 39.9‰ in January to 41.7‰ in September, with an increasing trend toward summer and decreasing trend toward winter and a seasonal variation of 1.8‰. The average value of $\delta^{18}O$ is 40.9‰. Based on the results of $\Delta'^{17}O$ values available, we got an average $\Delta'^{17}O$ values of -0.228‰$\pm$0.005‰(SE).

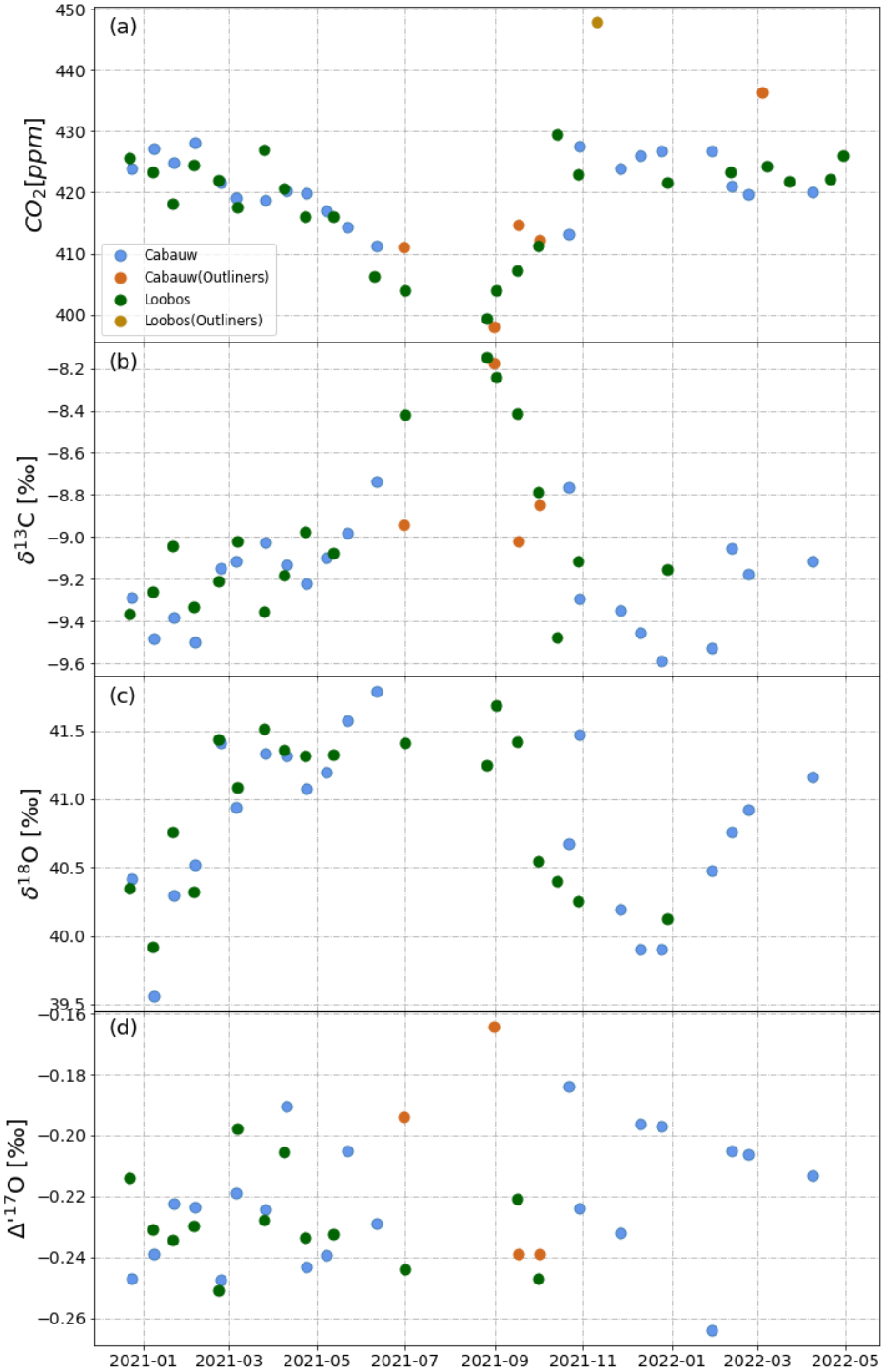

Figure 12: Temporal evolution of (a) CO_2 mole fraction [ppm], (b) $\delta^{13}C$ values [‰], (c) $\delta^{18}O$ values [‰] and (d) $\Delta'^{17}O$ values [‰] from December 2020 to April 2022 from Cabauw and Loobos. Blue points: results in Cabauw; Orange points: outliers in Cabauw; Green points: results in Loobos; Yellow points: Outliers in Loobos.

Sampling date	CO_2[ppm]	$\delta^{13}C$[‰]	$\delta^{18}O$[‰]	$\Delta'^{17}O$[‰]±[SE]
2020/12/23	424.0	-9.3	40.4	-0.247±0.006
2021/01/08	427.2	-9.5	39.6	-0.239±0.004
2021/01/22	424.9	-9.4	40.3	-0.222±0.005
2021/02/05	428.1	-9.5	40.5	-0.223±0.003
2021/02/23	421.6	-9.2	41.4	-0.247±0.006
2021/03/06	419.1	-9.1	40.9	-0.219±0.004
2021/03/26	418.7	-9.0	41.3	-0.224±0.004
2021/04/09	420.3	-9.1	41.3	-0.190±0.004
2021/04/23	419.9	-9.2	41.1	-0.243±0.006
2021/05/07	417.1	-9.1	41.2	-0.239±0.006
2021/05/21	414.4	-9.0	41.6	-0.205±0.007
2021/06/11	411.2	-8.7	41.8	-0.229±0.006
2021/06/29	411.2	-8.9	38.3	-0.194±0.007
2021/08/31	398.1	-8.2	29.7	-0.164±0.006
2021/09/17	414.7	-9.0	33.9	-0.239±0.005
2021/10/01	412.3	-8.8	39.6	-0.239±0.006
2021/10/22	413.3	-8.8	40.7	-0.184±0.004
2021/10/29	427.5	-9.3	41.5	-0.224±0.007
2021/11/26	424.0	-9.3	40.2	-0.232±0.006
2021/12/10	426.0	-9.5	39.9	-0.196±0.007
2021/12/24	426.8	-9.6	39.9	-0.197±0.007
2022/01/28	426.8	-9.5	40.5	-0.264±0.012
2022/02/11	421.1	-9.1	40.8	-0.205±0.006
2022/02/22	419.7	-9.2	40.9	-0.206±0.006
2022/03/04	436.3	-9.9	40.9	-0.213±0.007
2022/04/08	420.2	-9.1	41.2	-0.213±0.007
Average	421.5	-9.2	40.8	-0.221
Amplitude	17	0.9	2.2	0.08

Table 6. The sampling date, CO_2 mole fraction values, $\delta^{18}O$ values, $\delta^{13}C$ values and $\Delta'^{17}O$ values with standard error of CO_2 sampled in Cabauw from December 2020 to April 2022. The outliers are marked by grey shading.

Sampling date	CO_2[ppm]	$\delta^{13}C$[‰]	$\delta^{18}O$[‰]	$\Delta'^{17}O$[‰]±[SE]
2020/12/22	425.6	-9.4	40.3	-0.214±0.003
2021/01/07	423.4	-9.3	39.9	-0.231±0.004
2021/01/21	418.2	-9.0	40.8	-0.234±0.004
2021/02/04	424.6	-9.3	40.3	-0.230±0.005
2021/02/21	422.1	-9.2	41.4	-0.251±0.005
2021/03/06	417.6	-9.0	41.1	-0.198±0.004
2021/03/25	427.0	-9.4	41.5	-0.228±0.006
2021/04/08	420.7	-9.2	41.4	-0.205±0.006
2021/04/22	416.0	-9.0	41.3	-0.234±0.007
2021/05/12	416.1	-9.1	41.3	-0.232±0.007
2021/06/09	406.2	-	-	-
2021/06/30	403.9	-8.4	41.4	-0.244±0.006
2021/08/26	399.3	-8.2	41.3	-
2021/09/01	403.9	-8.2	41.7	-
2021/09/16	407.2	-8.4	41.4	-0.221±0.006
2021/09/30	411.2	-8.8	40.5	-0.247±0.006
2021/10/13	429.5	-9.5	40.4	-
2021/10/28	422.9	-9.1	40.3	-
2021/11/10	447.8	-10.3	40.3	-0.218±0.007
2021/12/28	421.6	-9.2	40.1	-
2022/02/10	423.4	-	-	-
2022/03/07	424.3	-	-	-
2022/03/23	421.8	-	-	-
2022/04/20	422.2	-	-	-
2022/04/29	426.0	-	-	-
Average	418.1	-9.0	40.9	-0.228
Amplitude	30	1.3	1.8	-

Table 7. The sampling date, CO_2 mole fraction values, $\delta^{18}O$ values, $\delta^{13}C$ values and $\Delta'^{17}O$ values with standard error of CO_2 sampled in Loobos from December 2020 to December 2021. The outliers are marked by grey shading.

5.2 Discussion

5.2.1 Potential reasons for biases

The four clear outliers in the period June to October for Cabauw may have been caused by several processes. The uncertainty of the sampling procedure may be one reason of these biases. The air samples taken during this period may have been contaminated during the sampling process. For example, the $Mg(ClO_4)_2$ in the dryer, which is used to reduce the moisture in the atmosphere before it went into the flasks, may have deteriorated when collecting the air sample, resulting in isotope exchange between the sample and moisture in the atmosphere. The outliers for $\delta^{18}O$ that scatter over a large range are most likely due to the isotope exchange with water.

The instability of the measurement system may be one source of some occasional large biases in observational results. Some outlier values of $\Delta'^{17}O$ from October 2021 to April 2022 may be due to the unstable CO_2 - O_2 exchange system. After few measurements, the CO_2 - O_2 exchange reactions couldn't reach equilibrium and the platinum catalyst was found out to be bad and replaced.

5.2.2 Comparison of observational data from Mace Head and Cabauw, Loobos: CO_2 mole fraction and $\delta^{13}C$

The observational data from Mace Head was chosen for comparison with the results from Cabauw and Loobos. Mace Head is close to the places we did the sampling and has similar climate conditions.

The CO_2 mole fraction values in Cabauw and Loobos from December 2020 to April 2022 are plotted together with data from Mace Head, County Galway, Ireland (MHD)) from January 2019 to December 2020 in Figure 13. The observation site data at Mace Head was retrieved from the databased of the Global Monitoring Laboratory of NOAA and shown as grey points. Comparing the two observation sites Cabauw and Loobos with Mace Head, they all show very similar seasonal patterns, with the minimum values of CO_2 mole fraction in summer and maximum values in winter. These seasonal patterns of the CO_2 concentration can be explained by the biospheric activities during the year. Plants take up more CO_2 through photosynthesis during summer, resulting in lower CO_2 concentration in the atmosphere from spring to summer. As many plants stop fixing CO_2 through photosynthesis from autumn to winter, CO_2 is released to the atmosphere through respiration. The data show CO_2 mole fraction values for Mace Head between 406 ppm in August 2021 and 425 ppm in January 2021, with a seasonal variation of around 19 ppm. This seasonal variation is very close to the result in Cabauw (~17 ppm), but lower than the results at Loobos (~30 ppm). Comparing these three locations, it can be seen that from 2019 to 2021, the CO_2 concentration increased steadily over years by around 5 ppm per year.

The (preliminary) $\delta^{13}C$ values from NOAA of the air sampled at Mace Head from January 2020 to April 2022 are plotted together with the results in Cabauw and Loobos from December 2020 to April 2022 in Figure 14. The numerical values of these preliminary data were not available, so the plots are merged together. The seasonal patterns of $\delta^{13}C$ values in Cabauw and Loobos are consistent with the data from Mace Head, all show an upward trend toward summer and decline toward winter. This seasonal pattern can be explained as follows: When plants absorb CO_2 through photosynthesis, they prefer to absorb ^{12}C over ^{13}C, resulting in more ^{13}C in the atmosphere when approaching summer. Focusing on the $\delta^{13}C$ from January 2021 to December 2021, Mace Head has the minimum value of $\delta^{13}C$ of approximately -9‰ and the maximum value of approximately -8.2‰, with a seasonal variation of around 0.8‰. The seasonal variation of $\delta^{13}C$ values in Cabauw(~1.1‰) and Loobos(~1.3‰) are slightly larger, with similar maximum values but lower minimum values compared to Mace Head.

There are various possible reasons leading to these seasonal variation difference between these sites. Different local ecosystems could be one of the reasons: Mace Head is a coastal measurement station on the west coast of Ireland, with the surrounding land being dominated by cropland; Cabauw in located in a grassland ecosystem, while Loobos located in a forest ecosystem, which would lead to differences in biosphere-atmosphere exchange and atmospheric conditions such as different local source of soil respiration. Besides, different sample collection times during a day as well as the different sample collection methods could also affect the results of the observations.

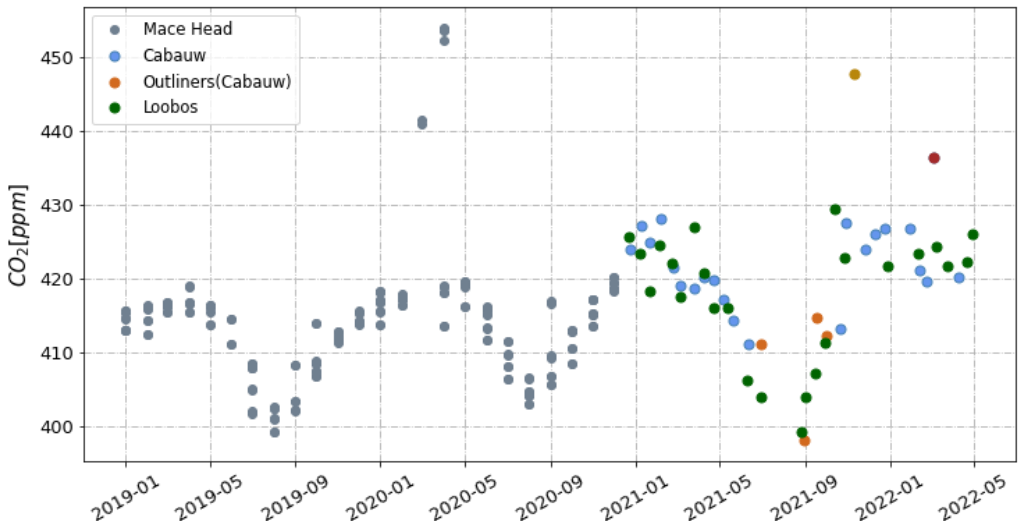

Figure 13: Temporal evolution of CO_2 mole fraction values [ppm] from the flask samples from 2019 to 2021 in Mace Head, County Galway, Ireland (MHD), adapted from https://gml.noaa.gov/dv/iadv/index.php. (grey points) and CO_2 mole fraction values [ppm] sampled at Cabauw (blue points) and Loobos (green points) from December 2020 to May 2022.

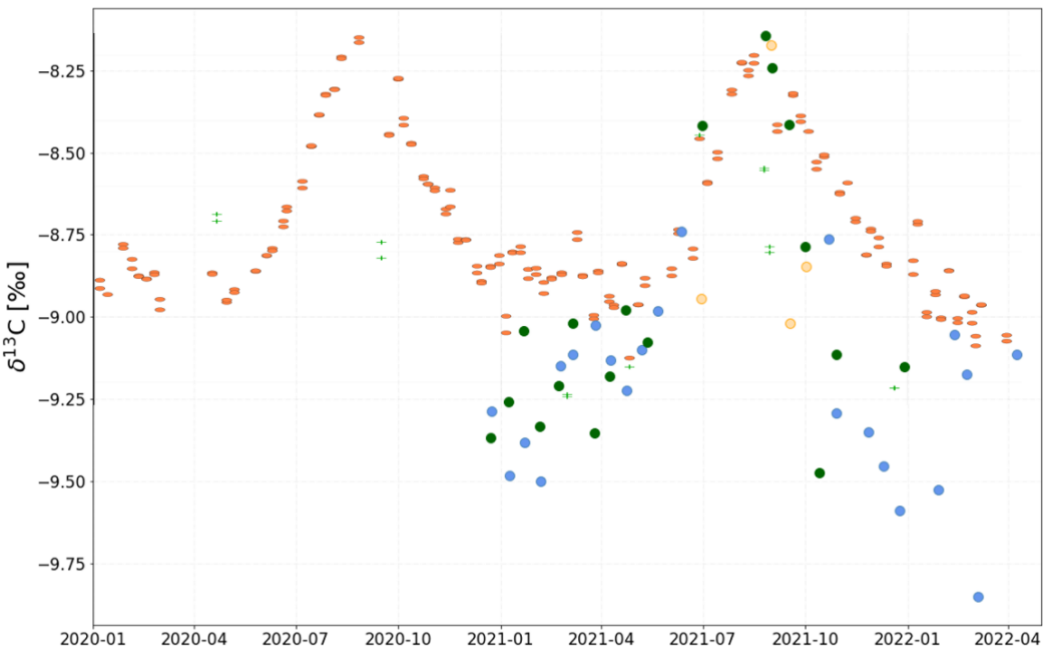

Figure 14: Comparison of the observation site data from Mace Head, Cabauw and Loobos, with temporal evolution of $\delta^{13}C$ values from the flask samples from 2019 to 2022 in Mace Head, County Galway, Ireland (MHD), adapted from https://gml.noaa.gov/dv/iadv/index.php. The data come from around weekly air samples collected in glass containers. The orange circles represent the preliminary data from year 2020 to 2022 from Mace Head. The green + symbols are considered to be poorly mixed air masses from Mace Head (e.g. impacted by anthropogenic sources; strong sources or sinks in the biosphere) that do not represent background conditions. The blue and green points represent the $\delta^{13}C$ values sampled in Cabauw and Loobos respectively.

5.2.3 Comparison of the different box model scenarios and the observations on $\Delta'^{17}O$ values

Melman, (2021) investigated the influence of different local factors on the $\Delta'^{17}O$ signal by using a box model. The lines for base run and experimental runs 1 to 8 shown in figure 15 represent $\Delta'^{17}O$ signal of different scenarios of the box model for two years' time series adapted from Melman, (2021). The results of the box model are based on the global 3D model by Koren et al. (2019). Experimental runs 1 to 8 represent different scenarios in order to investigate the influence of different local factors on the $\Delta'^{17}O$ signal. Experimental runs 1 and 2 represent the scenarios that GPP is reduced and amplified by 20% respectively and compensated by a change in ecosystem respiration (RE). Experimental runs 3 and 4 represent the scenarios that the perturbation of fossil fuel emission fluxes is compensated by increase and decrease of GPP respectively. Experimental runs 5 and 6 represent the scenarios that an altered fossil fuel emission flux is compensated by a change in the RE. Experimental runs 7 and 8 represent the scenarios that the changed fossil fuel emission flux is compensated by advection.

According to these output of difference scenarios, the $\Delta'^{17}O$ signals are generally lower in the cases of higher fossil fuel emission and higher GPP. The blue and green solid lines shown in figure 15 represent the results from Cabauw and Loobos. They are plotted together with the output of the box model in the second year to make a comparison.

According to these different scenarios of the box model, different local and regional factors can affect both the phase and amplitude of the $\Delta'^{17}O$ signal. Focusing on the model results for the second year, the $\Delta'^{17}O$ values increase toward July and approach their maximum values in spring or summer and then decreasing toward October for most of the scenarios, with average $\Delta'^{17}O$ values ranging from -0.221‰ to -0.136‰ and seasonal variations within 0.05‰. Focusing on the results in Cabauw, the $\Delta'^{17}O$ values show a slight upward trend toward summer and the maximum value is most possibly showing up between July and October. However, the minimum $\Delta'^{17}O$ values of different scenarios of the box model are reached in October and the maximum values are reached between April and July.

Comparing the average $\Delta'^{17}O$ values and their seasonal variation between the box model and observations from both Cabauw and Loobos, the average values in Cabauw (-0.221‰) and Loobos (-0.228‰) are closest to the output of experimental run 5 (-0.221‰), followed by the output of experimental run 7 (-0.217‰), which represent the scenarios of increased fossil fuel emission flux compensated by a change in the RE and compensated by advection respectively. The seasonal variation in Cabauw (0.08‰) is only slightly larger than the model results (ranging from 0.031‰ to 0.050‰). The results indicate that Cabauw and Loobos may have larger fossil fuel emission fluxes.

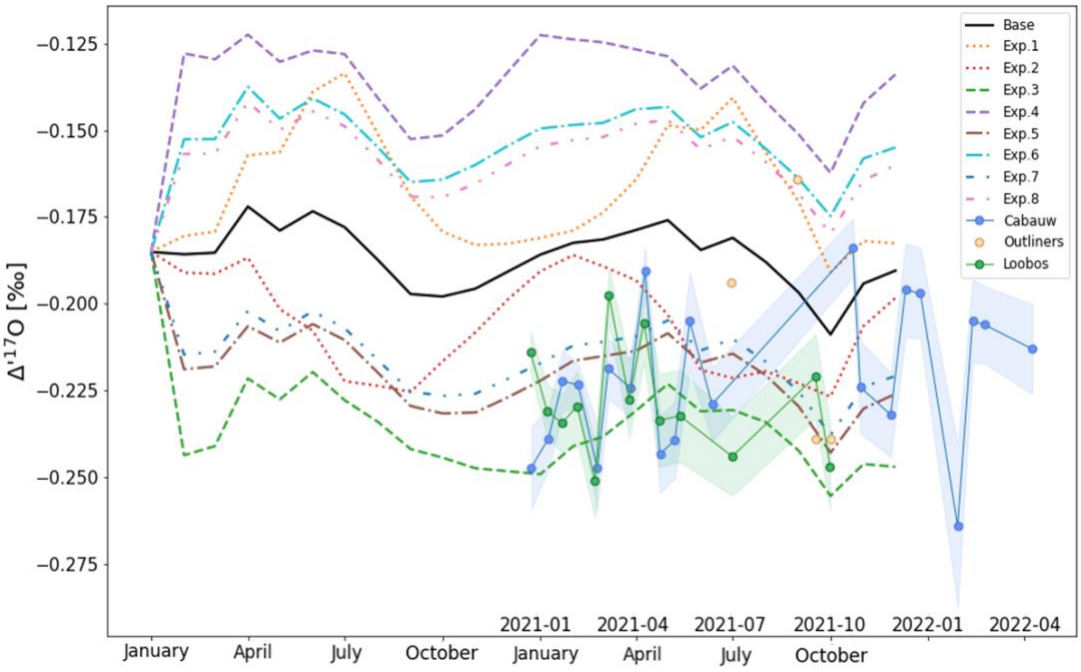

Figure 15: Comparison of $\Delta'^{17}O$ values of different box model scenarios for two years by Melman, (2021) and the observations in Cabauw and Loobos. The base run (black

line) is equal to the Global 3D TM model by Koren et al. (2019). Exp.1 to Exp.8 represent different scenarios of local factors. The blue and green solid lines represent the vertical average of $\Delta'^{17}O$ values in Cabauw and Loobos with their 95% confidence interval respectively. Outliers in Cabauw are shown in orange circles.

5.2.4 Comparison of different literature data and the observation on $\Delta'^{17}O$ values

Several previous studies have reported different average $\Delta'^{17}O$ values of troposphere CO_2 during different sampling periods in different observation locations.

Hofmann et al., 2017 reported the $\Delta'^{17}O$ values (relative to a reference slope of λ_{RL} = 0.5229) of ambient air CO_2 sampled in Göttingen, Germany for two years from 2010-2012, with a yearly average value of -0.02 ± 0.05‰(SD) in the first year, but with a very different yearly average value of -0.12 ± 0.04‰(SD) in the second year. In order to make the $\Delta'^{17}O$ values compatible with our results, the reference slope of λ_{RL} = 0.528 is used to recalculate these values. Therefore the yearly average value of $\Delta'^{17}O$ is equal to -0.245‰ in the first year and -0.326‰ in the second year. The $\Delta'^{17}O$ values show a seasonal pattern with maximum values in June/July and a seasonal amplitude of 0.13 ± 0.02‰, though the $\Delta'^{17}O$ signal is scattered.

Liang and Mahata (2015) reported an average $\Delta'^{17}O$ value (relative to a reference slope of λ_{RL} = 0.528) of -0.148‰ from near surface troposphere CO_2 sampled in Taiwan from September 2013 to February 2014, without clear seasonal pattern. Thiemens et al., 2014 reported an average $\Delta'^{17}O$ values (relative to a reference slope of λ_{RL} = 0.528) of -0.232‰ for troposphere CO_2 sampled in La Jolla, California from October 1990 to March 2000 but excluding the time period from 1997–1999 (due to the presence of extreme climatic event ENSO). The seasonal patterns are unclear according to the time series of $\Delta'^{17}O$ values.

Comparing the $\Delta'^{17}O$ values of these three literature studies with the data from Cabauw and Loobos, they all show very different average $\Delta'^{17}O$ values and seasonal variation. The average $\Delta'^{17}O$ values obtained in Göttingen are more depleted both for the first and second year compared to the result obtained in Cabauw (-0.221‰±0.006‰(SE)). The average $\Delta'^{17}O$ value obtained in La Jolla is more enriched compared to the result obtained in Cabauw. Meanwhile, most of these studies did not report a clear seasonal cycle and the results always scattered and changed a lot year by year.

The offset between these average $\Delta'^{17}O$ values of troposphere CO_2 could be attributed to several reasons. 1) One reason could be that different sampling sites are located in different ecosystems with different biosphere activity, therefore leading to different terrestrial assimilation flux and respiration flux rate. Cabauw may be influenced more by anthropogenic CO_2 emissions. 2) These $\Delta'^{17}O$ values of CO_2 are sampled in different time periods, varying from 1990 to 2022. During this large period, the

interannual variation of $\Delta'^{17}O$ values may be caused by increase anthropogenic CO_2 (CO_2 concentration rise year by year), biospheric activity, variation of the influx of stratospheric CO_2, etc. 3) There could be some measurement bias from varies procedures, and it's difficult to ensure precise and consistent measurements are performed at each step for each air sample. The $\Delta'^{17}O$ values are obtained by different CO_2 sampling methods and evaluated in different ways, which would also cause some deviation. 4) Some unexplained and unclear abnormal results, for example, $\Delta'^{17}O$ values of troposphere CO_2 sampled in Göttingen dropped around -0.1‰ from the first year to the second year. 5) The presence of extreme climatic event such as ENSO.

6 Conclusion

In this study, we investigated the stability and potential internal effects of CO_2-O_2 isotope exchange system for $\Delta'^{17}O$ measurement. The seasonal variation in the $\Delta'^{17}O$ value of troposphere CO_2 sampled in Cabauw and Loobos from December 2020 to April 2022 was determined by using isotope ratio mass spectrometry and CO_2-O_2 isotope exchange techniques.

- The analysis of $\Delta'^{17}O$ value of tropospheric CO_2 is carried out by a series of high precision procedures, including sample collection, CO_2 mole fraction measurement, CO_2 extraction, CO_2-O_2 isotope exchange reaction, CO_2-O_2 separation and determination of the $\Delta'^{17}O$, $\delta^{18}O$ and $\delta^{13}C$ values using an isotope ratio mass spectrometer.

- The time to reach isotope equilibrium for CO_2-O_2 isotope exchange was investigated. The time to reach equilibrium at a reactor temperature of 750℃ is not very sensitive to reactor pressures ranging from 57 to 120 mbar. The reaction approximately reaches the equilibrium state after 30 mins.

- The isotope effects of O_2 due to exchange with O in the quartz reactor at high temperature, and also with molecular sieve and silica gel were investigated. Freezing and releasing O_2 from both silica gel and molecular sieve affects $\delta^{17}O$ and $\delta^{18}O$, but the effect on $\Delta'^{17}O$ is negligible. Molecular sieve is the preferred material for trapping O_2 because the isotope effects on $\delta^{17}O$ and $\delta^{18}O$ are smaller than for silica gel.

- For the CO_2 - O_2 isotope exchange reaction, the isotope affect associated with thermal diffusion of isotopes between the hot and cold zones in the reactor was investigated. Larger thermal diffusion in the reactor will lead to smaller fractionation both for reactor temperature of 750℃ and 1000℃.

- Tropospheric CO_2 sampled in Cabauw and Loobos from December 2020 to April 2022 has an average CO_2 mole fraction of 421.5 ppm and 419.3 ppm respectively. The average values of $\delta^{13}C$ observed in Cabauw and Loobos are -9.2‰ and -9.0‰ respectively. The average values of $\delta^{18}O$ observed in Cabauw and Loobos are -40.8‰ and -40.9‰ respectively.

- Tropospheric CO_2 sampled in Cabauw has an average $\Delta'^{17}O$ value of 0.221‰ $\pm$ 0.008‰(SE) from December 2020 to April 2022. The temporal evaluation of $\Delta'^{17}O$ values indicates a small seasonal cycle with slight upward trend toward summer but a larger scatter during in the winter makes a clear definition of the seasonal cycle difficult. The seasonal amplitude is approximately 0.08 ‰, smaller than in previously published studies. The indicated seasonal variation of $\Delta'^{17}O$ with an upward trend toward summer would be a signal of an increase in the activity of terrestrial vegetation, so $\Delta'^{17}O$ may potentially be used as a tracer of GPP at the regional scale.

- Tropospheric CO_2 sampled in Loobos has an average $\Delta'^{17}O$ value of 0.228‰ from December 2020 to September 2021, without clear seasonal pattern.

- Part of the results of $\Delta'^{17}O$ values are scattered, these outliers could be attributed to the instability of the CO_2 - O_2 exchange system or contaminated air samples, etc. In order to better explain the seasonal cycles of $\Delta'^{17}O$ values of tropospheric CO_2 and get a better understanding of the connection between $\Delta'^{17}O$ and GPP, more observations for a longer time series in diverse ecosystems are needed in future work to minimize uncertainty.

Acknowledgements

I would like to express my appreciation to Thomas Röckmann, for his constant encouragement and guidance throughout this thesis. I would like to express my appreciation to Getachew Adnew for all his help and patience throughout this thesis, especially during the time he taught me measurement procedures in the laboratory. Moreover, I am grateful to meet APCG group members. I would like to express my appreciation to Carina, Elena, Marcel, Malu, Robert and many other people for all their support during the time I spent in the laboratory when I encountered difficulties.

Reference

1. Koren, G., Schneider, L., van der Velde, I. R., van Schaik, E., Gromov, S. S., Adnew, G. A., Mrozek Martino, D. J., Hofmann, M. E., Liang, M.-C., Mahata, S., et al. (2019). Global 3-d simu- lations of the triple oxygen isotope signature δ17o in atmospheric co2. Journal of Geophysical Re- search: Atmospheres, 124(15):8808–8836.

2. Luz, B. and Barkan, E. (2010). Variations of $^{17}o/^{16}o$ and $^{18}o/^{16}o$ in meteoric waters. Geochimica et Cosmochimica Acta, 74(22):6276– 6286.

3. Barkan, E., Musan, I., and Luz, B. (2015). High- precision measurements of $\delta^{17}o$ and ^{17}o excess of nbs19 and nbs18. Rapid Communications in Mass Spectrometry, 29(23):2219–2224.

4. Hoag, K., Still, C., Fung, I., and Boering, K. (2005). Triple oxygen isotope composition of tropospheric carbon dioxide as a tracer of terrestrial gross carbon fluxes. Geophysical Research Let- ters, 32(2).

5. Liang, M.-C., Mahata, S., Laskar, A. H., Thiemens, M. H., and Newman, S. (2017). Oxygen isotope anomaly in tropospheric co2 and implications for co2 residence time in the atmosphere and gross primary productivity. Scientific reports, 7(1):1– 12.

6. Mahata, S., Bhattacharya, S., Wang, C.-H., and Liang, M.-C. (2013). Oxygen isotope exchange between o2 and co2 over hot platinum: An innovative technique for measuring δ17o in co2. Analytical chemistry, 85(14):6894–6901.

7. Adnew, Getachew A et al. (2019). Determination of the triple oxygen and carbon isotopic composition of CO2 from atomic ion fragments formed in the ion source of the 253 Ultra high-resolution isotope ratio mass spectrometer. Rapid Communications in Mass Spectrometry 33.17, pp. 1363–1380.

8. Meijer, H. & Li, W. (1998). The use of electrolysis for accurate delta O-17 and delta O-18 isotope measurements in water. Isotopes in Environmental and Health Studies 34(4), 349–369.

9. G.A. Adnew., E. Workman., C. Janssen., T. Röckmann. (2021), Temperature dependence of the isotopic fractionation in the CO2 - O2 isotope exchange reaction. Rapid Communications in Mass Spectrometry

10. Hofmann, M., Horváth, B., Schneider, L., Peters, W., Schützenmeister, K., and Pack, A. (2017). Atmospheric measurements of δ17o in co2 in göt- tingen, germany reveal a seasonal cycle driven by biospheric uptake. Geochimica et Cosmochimica Acta, 199:143–163.

11. Yan H, Peng Y, Bao H. Isotope fractionation during capillary leaking in an isotope ratio mass spectrometer. Rapid Commun Mass Spectrom. 2022 Mar 8:e9290. doi: 10.1002/rcm.9290. Epub ahead of print. PMID: 35261096.

12. Joiner, J., Yoshida, Y., Zhang, Y., Duveiller, G., Jung, M., Lyapustin, A., Wang, Y., and Tucker, C. J. (2018). Estimation of terrestrial global gross primary production (gpp) with satellite data- driven models and eddy covariance flux data. Re- mote Sensing, 10(9):1346.

13. Booth, B. B. B., Jones, C. D., Collins, M., Totterdell, I. J., Cox, P. M., Sitch, S., et al. (2012). High sensitivity of future global warming to land carbon cycle processes. Environmental Research Letters, 7(2), 024002. https://doi.org/10.1088/1748-9326/7/2/024002

14. Liang, MC., Mahata, S. Oxygen anomaly in near surface carbon dioxide reveals deep stratospheric intrusion. Sci Rep 5, 11352 (2015). https://doi.org/10.1038/srep11352

15. I.C. Prentice, G.D. Farquhar, M.J.R. Fasham, M.L. Goulden, M. Heimann, et al.. The carbon cycle and atmospheric carbon dioxide. Climate change 2001: the scientific basis, Intergovernmental panel on climate change, 2001. hal-03333974

16. Le Quéré, C., Andrew, R. M., Friedlingstein, P., Sitch, S., Hauck, J., Pongratz, J., Pickers, P. A., Korsbakken, J. I., Peters, G. P., Canadell, J. G., et al. (2018). Global carbon budget 2018. Earth System Science Data, 10(4):2141–2194.

17. Beer, C. et al. Terrestrial Gross Carbon Dioxide Uptake: Global Distribution and Covariation with Climate. Science 329, 834–838 (2010).

18. Gurney, K. R., et al. (2002), Towards robust regional estimates of CO2 sources and sinks using atmospheric transport models, Nature, 415, 626 – 630.

19. Farquhar, G. D., Lloyd, J., Taylor, J. A., Flanagan, L. B., Syvertsen, J. P., Hubick, K. T., Wong, S. C. & Ehleringer, J. R. (1993), 'Vegetation Effects on the Isotope Composition of Oxygen in Atmospheric CO2', Nature 363, 439–443.

20. Ciais, P., Denning, A. S., Tans, P. P., Berry, J. A., Randall, D. A., Collatz, G. J., Sellers, P. J., White, J. W. C., Trolier, M., Meijer, H. A. J. & et al. (1997), 'A Three-dimensional Synthesis Study of δ18O in Atmospheric CO2: 1. Surface Fluxesd', Journal of Geophysical Research: Atmospheres 102(D5), 5857–5872.

21. Francey, R. J. & Tans, P. P. (1987), 'Latitudinal Variation in Oxygen-18 of Atmospheric CO2', Nature 327(6122), 495–497.

22. Liang, M.-C., G. A. Blake, and Y. L. Yung (2008), Seasonal cycle of C16O16O, C16O17O, and C16O18O in the middle atmosphere: Implications for mesospheric dynamics and biogeochemical sources and sinks of CO2, J. Geophys. Res., 113, D12305, doi:10.1029/2007JD008392.

23. Luz B, Barkan E, Bender ML, Thiemens MK, Boering KA. Triple-isotope composition of atmospheric oxygen as a tracer of biosphere productivity. Nature. 1999;400(6744):547-550. doi:10.1038/22987

24. Prosenjit Ghosh, Willi A. Brand. (2004), The effect of N2O on the isotopic composition of air-CO2 samples. Rapid Communications in Mass Spectrometry 18(16):1830-1838.

25. S. S. Assonov, C. A. M. Brenninkmeijer, On the N2O correction used for mass spectrometric analysis of atmospheric CO2, Rapid Communications in Mass Spectrometry, 10.1002/rcm.2516, 20, 11, (1809-1819), (2006).

26. Z. Gorczyca, M. Piasecka, The N2O correction in mass-spectrometric analysis of CO2, NUKLEONIKA 2004;49(2):37−42

27. Thiemens M. H., Chakraborty S. and Jackson T. L. (2014) Decadal D17O record of tropospheric CO2: verification of a stratospheric component in the troposphere. J. Geophys. Res. Atmos. 119, 2013JD020317.

28. E.A. Melman. (2021) Seasonal and diurnal evolution of triple-oxygen isotopes in CO2 above three different ecosystems.